UNIVERSIDADE ESTADUAL PAULISTA - UNESP
CÂMPUS DE JABOTICABAL

PHYSIOLOGICAL AND SPECTRAL RESPONSES OF SUGARCANE TO THE INJURY OF SUGARCANE BORERS: BASIS FOR ENHANCING PEST MONITORING

João Rafael Silva Soares
Agronomist Engineer

2024

UNIVERSIDADE ESTADUAL PAULISTA - UNESP
CÂMPUS DE JABOTICABAL

PHYSIOLOGICAL AND SPECTRAL RESPONSES OF SUGARCANE TO THE INJURY OF SUGARCANE BORERS: BASIS FOR ENHANCING PEST MONITORING

Student: João Rafael Silva Soares
Advisor: Prof. Dr. Odair Aparecido Fernandes

Thesis presented to the School of Agricultural and Veterinary Sciences – São Paulo State University (Unesp), Jaboticabal Campus, as part of requirements to obtain the Doctorate degree in Agronomy (Agricultural Entomology)

2024

S676p

Soares, João Rafael Silva
Physiological and spectral responses of sugarcane to the injury of sugarcane borers: basis for enhancing pest monitoring / João Rafael Silva Soares. -- Jaboticabal, 2024
77 p. : il., tabs., fotos, mapas

Tese (doutorado) - Universidade Estadual Paulista (UNESP), Faculdade de Ciências Agrárias e Veterinárias, Jaboticabal
Orientador: Odair Aparecido Fernandes

1. Agricultura de precisão. 2. Machine learning. 3. Monitoramento. 4. Tomada de decisões. 5. Sensoriamento remoto. I. Título.

Sistema de geração automática de fichas catalográficas da Unesp. Dados fornecidos pelo autor(a).

UNIVERSIDADE ESTADUAL PAULISTA

Câmpus de Jaboticabal

CERTIFICADO DE APROVAÇÃO

TÍTULO DA TESE: PHYSIOLOGICAL AND SPECTRAL RESPONSES OF SUGARCANE TO THE INJURY OF SUGARCANE BORERS: BASIS FOR ENHANCING PEST MONITORING

AUTOR: JOÃO RAFAEL SILVA SOARES

ORIENTADOR: ODAIR APARECIDO FERNANDES

Aprovado como parte das exigências para obtenção do Título de Doutor em Agronomia (Entomologia Agrícola), pela Comissão Examinadora:

gov.br Documento assinado digitalmente
ODAIR APARECIDO FERNANDES
Data: 25/09/2024 09:36:04-0300
Verifique em https://validar.iti.gov.br

Prof. Dr. ODAIR APARECIDO FERNANDES (Participaçao Presencial)
Departamento de Fitossanidade / FCAV UNESP Jaboticabal

gov.br Documento assinado digitalmente
LUCAS RIOS DO AMARAL
Data: 25/09/2024 09:05:42-0300
Verifique em https://validar.iti.gov.br

Prof. Dr. LUCAS RIOS DO AMARAL (Participaçao Virtual)
Faculdade de Engenharia Agrícola / Universidade Estadual de Campinas (UNICAMP) - Campinas/SP

Prof. Dr. GUILHERME DUARTE ROSSI (Participaçao Presencial)
Departamento de Fitossanidade / FCAV UNESP Jaboticabal

gov.br Documento assinado digitalmente
GUILHERME DUARTE ROSSI
Data: 24/09/2024 14:07:49-0300
Verifique em https://validar.iti.gov.br

Pesquisador Dr. JAYME GARCIA ARNAL BARBEDO (Participaçao Virtual)
Departamento de Computação Científica, Engenharia de Informação e Automação / Embrapa Agricultura Digital - Campina/SP

gov.br Documento assinado digitalmente
JAYME GARCIA ARNAL BARBEDO
Data: 25/09/2024 08:59:37-0300
Verifique em https://validar.iti.gov.br

Pós-Doutorando RODRIGO CUPERTINO BERNARDES (Participaçao Presencial)
Departamento de Fitossanidade / FCAV UNESP Jaboticabal

gov.br Documento assinado digitalmente
RODRIGO CUPERTINO BERNARDES
Data: 25/09/2024 09:11:20-0300
Verifique em https://validar.iti.gov.br

Jaboticabal, 20 de setembro de 2024

DADOS CURRICULARES DO AUTOR

JOÃO RAFAEL SILVA SOARES nasceu em 18 de dezembro de 1992, em Pompéu – MG. É filho de Francisco Lino Soares Bisneto e Sônia Martinha da Silva Soares. Formou-se Engenheiro Agrônomo pela Universidade Federal de Viçosa (UFV), campus Viçosa, título obtido em janeiro de 2018. Foi estagiário do Laboratório de Manejo Integrado de Pragas da UFV, sob a supervisão do professor Marcelo Coutinho Picanço, onde desenvolveu projetos de iniciação científica com bolsa FUNAPE-Embrapa Café durante a graduação. Ainda durante a graduação foi agraciado com uma bolsa pelo programa Ciências sem Fronteiras, fornecida pela Coordenadoria de Aperfeiçoamento Pessoal de Nível Superior (CAPES), permanecendo na Michigan State University por 1,5 anos. Foi aprovado para cursar o mestrado em Fitotecnia pela UFV – campus Viçosa, sob a orientação do Prof. Dr. Marcelo Coutinho Picanço em fevereiro de 2018. Em janeiro de 2020, foi aprovado para cursar o Doutorado em Agronomia (Entomologia Agrícola) na Faculdade de Ciências Agrárias e Veterinárias da Universidade Estadual Paulista (Unesp) – câmpus Jaboticabal, sob a orientação do Prof. Dr. Odair Aparecido Fernandes, na qual teve a oportunidade de aprofundar seus conhecimentos sobre Manejo Integrado de Pragas de grandes culturas, especialmente pragas da cana-de-açúcar.

AUTHOR'S CURRICULUM DATA

JOÃO RAFAEL SILVA SOARES was born on December 18, 1992, in Pompéu, Minas Gerais state, Brazil. He is the son of Francisco Lino Soares Bisneto and Sônia Martinha da Silva Soares. In January 2018, he graduated as an agronomist at the Federal University of Viçosa (UFV), Viçosa Campus. During his undergraduate studies, he was an intern at the UFV Laboratory for Integrated Pest Management, under the supervision of Professor Dr. Marcelo Coutinho Picanço, where he developed scientific projects with FUNAPE - Embrapa Café (Embrapa coffee). He was awarded a scholarship for the Science Without Borders program, provided by the Coordenação de Aperfeiçoamento de Pessoal de Nível Superior (CAPES), and stayed at Michigan State University for 1.5 years. The UFV-Viçosa campus approved his master's degree in Plant Science in February 2018, under the supervision of Prof. Dr. Marcelo Coutinho Picanço.In January 2020, he was approved to pursue a doctorate degree in Agronomy (Agricultural Entomology) at the School of Agricultural and Veterinary Sciences of São Paulo State University (Unesp) Jaboticabal campus, under the supervision of Prof. Dr. Odair Aparecido Fernandes, in which he had the opportunity to deepen his knowledge on integrated pest management of field crops, especially sugarcane pests.

“If you think education is expensive, try ignorance.”

Derek Bok, former president of Harvard University

To my dear and beloved family. Especially my mother, Sônia Martinha da Silva Soares, who was my greatest encourager and great example of moral and affective conduct,

I dedicate.

ACKNOWLEDGEMENTS

To God almighty for allowing me to conquer another great victory in my life.

To my family, especially my mother Sônia, my father Francisco, brother Gabriel, and sisters Jaqueline and Jeany, for backing up my decisions to pursue a higher education degree and being a source of energy replenishment during my “dog days” along my academic career.

A special thanks to Claudiane, for filling me with love and making my days during my doctorate journey happier! Thank you for your partnership, affection, patience, and encouragement.

To the Faculty of Agricultural and Veterinary Sciences of the São Paulo State University for the infrastructure and opportunity granted.

To the teachers of the Postgraduate Degree in Agronomy/Agricultural Entomology, for transmitted knowledge.

A special thank you to all the Applied Ecology Laboratory (ApEcoLab) colleagues, especially Vinícius Cesarin, Rafaela Martin, Julia Karoline, Beliza Queiroz, Marina Brum de Castro, Luís Augusto Gervásio Junqueira, and Juliana Vieira for the help in conducting the experiments.

To colleagues from other laboratories, Joacir do Nascimento, Daniel Dalvan, and Juliana Queiroz for the casual talks.

To the staff of the Department of Plant Health, in particular to André Maurício Múscari, Alex Antônio Ribeiro, Cibele da Silva Anton, and Zulene Antônio Ribeiro for the many aids provided.

To Professor Dr. Odair Aparecido Fernandes for his teachings and guidance during my doctorate degree.

To the professors Dr. Nilton Nobuhiro Imai, Antônio Maria Garcia Tommaselli, Fernanda Sayuri Yoshino Watanabe, and Priscila Lupino Gratão for their knowledge and enriching discussions about my project.

To the Foundation for Research Support of the State of São Paulo (FAPESP 2021/09645-0) and the Coordenação de Aperfeiçoamento de Pessoal de Nível Superior (CAPES) – Finance Code 001 for the granting of the scholarship and support that enabled

to conduct the proposed project. This work is associated with the Center for Research in Engineering – Plant Health in Sugarcane - CEPENFITO (FAPESP 2017/25258-1). This study was financed in part by the Coordenação de Aperfeiçoamento de Pessoal de Nível Superior - Brasil (CAPES) - Finance Code 001.

TABLE OF CONTENTS

Page

CHAPTER 1 – General considerations 1

References 5

CHAPTER 2 – Interaction between water deficit and injury of sugarcane borer (Lepidoptera: Crambidae) in the gas exchange parameters and spectral reflectance of the sugarcane 8

Resumo 8

Abstract 9

Introduction 10

Materials and Methods 12

Plants 12

Experimental design 12

Gas exchange measurements 13

Foliar spectral measurements 14

Data analysis 15

Results 18

Influence of the combination of stressors on sugarcane gas exchange parameters 18

Water regime and sugarcane borer combination on sugarcane spectral reflectance 21

Discussion 22

References 26

CHAPTER 3 – Comparison of multispectral remote sensing platforms for sugarcane billbug attack (Coleoptera: Curculionidae) detection: a proposal for sampling optimization 36

Resumo 36

Abstract 37

Introduction 38

Materials and Methods 39

Multispectral UAV image acquisition 42

Multispectral satellite image acquisition 43

Image and vector files processing 44

Data processing, analysis and implementation of machine learning models 49

Results 53

Sugarcane billbug damage dynamics, population and cumulative progress of attack 53

UAV remote sensing 54
Orbital remote sensing 60
Discussion 66
References 70
CHAPTER 4 – Concluding remarks 76

RESPOSTAS FISIOLÓGICAS E ESPECTRAIS DA CANA-DE-AÇÚCAR ÀS INJÚRIAS CAUSADAS POR FITÓFAGOS BROQUEDORES: BASES PARA A MELHORIA DO MONITORAMENTO DE PRAGAS

RESUMO – O monitoramento de pragas é essencial para programas de Manejo Integrado de Pragas (MIP), pois permite a detecção precoce de infestações e auxilia na tomada de decisão para a implementação de estratégias de controle. No entanto, muitos estudos ainda negligenciam as interações entre pragas e outros fatores estressores, como os abióticos, que podem agravar os prejuízos ao desenvolvimento das plantas. Na cultura da cana-de-açúcar, pragas como a broca-da-cana e o bicudo-da-cana causam perdas significativas, especialmente em condições de estresse hídrico. Técnicas emergentes, como o sensoriamento remoto, que utiliza sensores para detectar mudanças fisiológicas nas plantas, mostram-se promissoras para o monitoramento de pragas. Este estudo explora como as infestações dessas pragas afetam as respostas fisiológicas e espectrais da cana-de-açúcar e investiga a eficácia de sensores multiespectrais para detectar alterações na reflectância espectral das plantas causados pelo bicudo-da-cana. Inicialmente, foi investigado em casa-de-vegetação, como a infestação pela broca-da-cana e diferentes regimes hídricos alteram parâmetros de trocas gasosas e a reflectância espectral da cana-de-açúcar. Posteriormente, foi realizado monitoramento mensal de áreas experimentais infestadas com o bicudo-da-cana em canaviais comerciais. A resposta espectral das plantas foi registrada por sensores multiespectrais embarcados em veículos aéreos não tripulados (VANTs) e satélites. Os resultados revelaram que tanto o déficit hídrico quanto a infestação pela broca-da-cana, isolados ou combinados, afetam significativamente parâmetros como transpiração (E), condutância estomática (gs) e fotossíntese líquida (A), dificultando a distinção entre os efeitos da broca-da-cana e os causados pelo déficit hídrico. As respostas das variedades de cana diferiram, com a variedade tolerante ao estresse hídrico apresentando menores valores para os parâmetros gasosos, sugerindo interações complexas entre a fisiologia da planta e os estressores. Além disso, a detecção do ataque da broca-da-cana via sensoriamento remoto mostrou-se desafiadora, com os algoritmos de *machine learning* (ML) apresentando dificuldades em distinguir corretamente os estresses. No monitoramento do bicudo-da-cana, foi identificada uma relação significativa entre os níveis de infestação e a reflectância espectral das plantas, variando conforme a variedade de cana e o nível de infestação. Os modelos de ML foram eficazes ao estimar a intensidade de ataque acumulado, especialmente quando os dados consideraram a fase de crescimento da cana e a fase danosa da praga, sendo os algoritmos de árvores de decisão os mais eficientes. A análise também destacou a importância de bandas espectrais específicas e índices de vegetação como o MCARI, sensíveis às alterações causadas pelo ataque do bicudo-da-cana. Surpreendentemente, os dados provenientes de satélites superaram os VANTs em termos de poder preditivo. Esses achados reforçam a necessidade de considerar a tolerância da cana a múltiplos estressores na estimativa de limiares econômicos de dano e apontam para a incorporação de ferramentas digitais como uma abordagem promissora para o monitoramento em larga escala do bicudo-da-cana.

PALAVRAS-CHAVE: Agricultura de precisão, *Diatraea saccharalis*, Ecofisiologia, Monitoramento inteligente, Tomada de decisão, Sensoriamento remoto, *Sphenophorus levis*.

PHYSIOLOGICAL AND SPECTRAL RESPONSES OF SUGARCANE TO THE INJURY OF SUGARCANE BORERS: BASIS FOR ENHANCING PEST MONITORING

ABSTRACT – Pest monitoring is essential for Integrated Pest Management (IPM) programs, as it allows early detection of pest infestations and aids decision-making for the implementation of control strategies. However, many studies still neglect the interactions between pests and other stressors, such as abiotic ones, which can aggravate plant damage. Pests in sugarcane crops, such as the sugarcane borer and the sugarcane billbug, cause significant losses, especially under water shortage conditions. Emerging techniques, such as remote sensing, which uses sensors to detect physiological changes in plants, show promise for pest monitoring. This study explores the impact of pest infestations on the physiological and spectral responses of sugarcane, as well as the efficacy of multispectral sensors in identifying damage from the sugarcane billbug. Initially, it was investigated how sugarcane borer infestation and different water regimes alter gas exchange parameters and spectral reflectance of sugarcane under semi-field conditions. Subsequently, monthly monitoring of sugarcane billbug was carried out in experimental areas infested with this pest in commercial sugarcane fields. Multispectral sensors on board unmanned aerial vehicles (UAVs) and satellites recorded the spectral response of the plants. The results revealed that both water deficit and sugarcane borer infestation, isolated or combined, significantly affect parameters such as transpiration (E), stomatal conductance (gs), and net photosynthesis (A), making it difficult to distinguish between the effects of the sugarcane borer and those caused by water deficit. The responses of sugarcane varieties differed, with the drought-tolerant variety presenting lower values for gas exchange parameters, suggesting complex interactions between plant physiology and stressors. Furthermore, detecting sugarcane borer attacks via remote sensing proved challenging, with machine learning (ML) algorithms struggling to correctly distinguish stresses. In sugarcane billbug monitoring, a significant relationship was identified between infestation levels and plant spectral reflectance, varying according to sugarcane variety and infestation level. ML models were effective in estimating the intensity of the accumulated attack, especially when the data considered the sugarcane growth phase and the damage phase of the pest, with decision tree algorithms being the most efficient. The analysis also highlighted the importance of specific spectral bands and vegetation indices, such as MCARI, which are sensitive to changes caused by sugarcane billbug attacks. Surprisingly, satellite data outperformed UAVs in terms of predictive power. These findings reinforce the need to consider sugarcane tolerance to multiple stressors when estimating economic damage thresholds, and they point to the incorporation of digital tools as a promising approach for large-scale monitoring of the sugarcane billbug.

KEYWORDS: *Diatraea saccharalis*, Decision making, Ecophysiology, Precision agriculture, Remote sensing, Smart monitoring, *Sphenophorus levis*.

CHAPTER 1 – General considerations

Pest monitoring is one of the key pillars of the Integrated Pest Management Program (IPM). At this stage, quantitative and qualitative data are collected that support decision-making, enabling the implementation of more efficient and cost-effective management strategies and tactics (Pedigo, Hutchins and Higley, 1986; Dara, 2019). By detecting pests in the early stages of infestation, monitoring enables early interventions, preventing severe damage and consequently significant economic losses (Higley and Pedigo, 1996).

The development of precise sampling plans requires in-depth studies of how pest insects affect plants to accurately identify infestation signs, and the specific damage caused (Peterson, Higley and Pedigo, 2018). However, most studies evaluating the impact of pest-induced stress neglect the potential interactions with other stressors (Pandey *et al.*, 2017). This is often contrary to what happens in natural conditions, in which multiple stressors act simultaneously or in succession (Zandalinas *et al.*, 2024). The combination of biotic stresses (caused by living beings) and abiotic stresses (prompted by non-living environmental factors), for example, can have synergistic effects, increasing the total negative impacts on the plant (Zandalinas and Mittler, 2022). Plants subjected to a prior stressor can modulate the behavior of herbivories, such as food preferences and oviposition sites. In addition, abiotic stresses can weaken plant natural defenses, making them more susceptible to pests (Lynch, 2022; Zandalinas and Mittler, 2022).

Sugarcane (*Saccharum* spp.) is one of the most important crops for the Brazilian economy due to its diversity of applications. Brazil is the world's largest sugar producer and the second largest ethanol producer, with an estimated production of 45 million tons of sugar and 30 billion liters of ethanol on a cultivated area of 8,333.90 thousand ha (Conab, 2024). São Paulo state accounts for 49.1% of the cultivated area, with an average yield of approximately 92 tons ha^{-1} in 2023, making it the largest national grower (Conab, 2024). Although the country gains prominence as one of the largest sugarcane cultivated areas and yield, the losses caused by stress agents refrain the sector from achieving higher yield levels.

Water restriction is the most restrictive abiotic stress for sugarcane yield among the stressors (Dlamini, 2021). Under water deficit, plants retain water to balance their

use, but at the cost of reducing the capture of CO_2 and, consequently, the carbon fixation in metabolic processes due to the closure of the stomates (Inman-Bamber, Lakshmanan and Park, 2012; Hussain *et al.*, 2018).

Pest infestations such as the sugarcane borer *Diatraea saccharalis* (Fabricius, 1794) (Lepidoptera: Crambidae) and the sugarcane billbug *Sphenophorus levis* Vaurie, 1978 (Coleoptera, Curculionidae) are examples of biotic stressors and stand out as the most important insect pests in São Paulo sugarcane fields. The presence of a sugarcane borer can reduce the weight and quality of the culms, directly affecting the production of sugar and the quality of raw materials (Rossato *et al.*, 2013). Once the larvae enter the culm, they leave a hole that allows opportunistic fungi from the red rot complex, such as *Fusarium* spp. and *Colletotrichum* spp., to enter. These fungi cause the inversion of the sucrosis and reduce the industrial quality (Rossato *et al.*, 2013). In recent years, the sugarcane billbug *Sphenophorus levis* Vaurie, 1978 (Coleoptera: Curculionidae) have become one of the main pests in sugarcane (Xavier *et al.*, 2024). The larvae bore the base of the culms, causing progressive yellowing and can lead the plants to death (Dinardo-Miranda, 2005). The attack reduces the diameter, length, and number of culms, especially in dry seasons, decreasing sugarcane longevity and yield (Xavier *et al.*, 2024).

Decision-making for control of these pests is based on population surveys *in loco*. For the sugarcane borer, two sampling schemes are proposed. A direct visual inspection is carried out on two sugarcane cultivation lines with five meters each to make an average estimative of the number and development stage of the sugarcane borer larvae. However, monitoring based on delta traps containing virgin females, which release sexual pheromones to attract males, has recently emerged as an interesting option for farmers, as it makes possible to start control of eggs and larvae before boring into culms. The monitoring of the sugarcane billbug requires scouters to remove the clump from the soil with a mattock and inspect the remains of the culms, popularly known as stumps, to count injuries and any developmental stages of the insect, i.e., larvae, pupae, and adults (Dinardo-Miranda, 2005; Xavier *et al.*, 2024).

Due to the laborious nature of conventional sampling plans, walking through sugarcane fields to visually evaluate the presence of insects or their injuries is inefficient and often impractical, especially for companies (sugarcane millers and distilleries) or growers with large areas and limited labor availability. Meanwhile, in an age of intense digitization of agriculture, remote sensing can optimize pest monitoring

efficiency and speed up decision-making (Nansen, 2016). Remote sensing consists of obtaining information about objects or areas at a distance without the need for direct physical contact (Jensen, 2007). Advances in sensor technology, such as radar, multispectral, and hyperspectral, offer new opportunities for application in different farming systems (Zhang *et al.*, 2019). Currently, these sensors are classified into active and passive sensors (Toth and Jóźków, 2016). Active sensors emit their own electromagnetic radiation, such as radio waves, microwaves, or light, and then measure the reflected or spread radiation by objects (Jensen, 2007). In contrast, passive sensors do not emit any signals; they only measure the radiation that is reflected, transmitted, or naturally emitted by the targets (Jensen, 2007). Both sensor types have specific applications and are chosen based on the needs of the remote sensing project (Toth and Jóźków, 2016). However, the lower cost of acquisition, data processing, and maintenance often leads to the preference for passive sensors (Zhang *et al.*, 2021).

Herbivory stress triggers a physiological defense response in plants, resulting in changes in foliar reflectance, making pest detection through remote sensing feasible (Zhang *et al.*, 2019). Biochemical changes during plant growth, such as the concentration of chlorophyll and water, affect the amount of electromagnetic radiation reflected, absorbed, or transmitted by plants (Nansen and Elliott, 2016). These changes can be observed through manual terrestrial sensors or coupled to platforms such as robots, vehicles, unmanned aerial vehicles (UAVs), airplanes, and satellites, allowing the detection of spatial and/or temporal anomalies in agricultural fields (Toth and Jóźków, 2016).

Strategies inserted in the Digital Agriculture, such as the integration of different sensors, processing systems, and data handling, assist in the manipulation of big data databases (Barbedo, 2023). Furthermore, artificial intelligence (AI) algorithms allow digital image processing and the extraction of features of interest (Barbedo, 2023; Shaikh, Rasool and Lone, 2022; Zhang *et al.*, 2019).

Machine learning (ML) is a subfield of AI in which algorithms have a high ability to recognize patterns from data (learning) and can be accurate in identifying pests or symptoms of attack in their hosts (Shinde and Shah, 2018). ML algorithms can therefore identify patterns in the raw data and extract significant information from it. Machine learning techniques have two fundamental tasks (Behmann *et al.*, 2015). Unsupervised learning begins with unlabeled data and searches for unidentified

patterns that enable the creation of a new, more condensed, or more thorough representation of the information it contains (Attri, Awasthi e Sharma, 2024). The most well-known use of unsupervised learning is clustering, which is the process of organizing data instances into various clusters. Clustering methods typically create groups of samples with comparable characteristics throughout the whole dataset. Supervised learning techniques can be used if target variables with label names “y”, and the predictors are available (Bishop 2006). In this case, it is crucial to find patterns in the data that are connected to the labels (this enables the prediction of previously undiscovered new data) (Attri, Awasthi and Sharma, 2024).

The purpose of the application should guide the selection of the best machine learning data analysis technique (Shinde and Shah, 2018). As such, generic recommendations are not attainable, although some criteria can be used to find relevant algorithms. A few fundamental characteristics are crucial for choosing a method such as the quantity of features, the quantity of training samples, the nature of the label, and details regarding the data distributions (Behmann *et al.*, 2015). A supervised approach ought to be employed, presuming that the label information is supplied (Zubler and Yoon, 2020). One can only employ unsupervised approaches in the absence of labels. Regression is needed for continuous label values, while classification is needed for discrete ones (Zubler and Yoon, 2020). Artificial neural networks (ANNs), support vector machines (SVMs), random forests (RFs), and K-means clustering are a few of the most widely used machine learning techniques used for both classification or regression purposes, while K-means also can be used as clustering method (Attri, Awasthi and Sharma, 2024; Behmann *et al.*, 2015).

As in other crops, the sugarcane agroecosystem faces several stressors whose effects may be difficult to identify and quantify. Therefore, the similarity of injuries caused by biotic and abiotic agents, the genetic composition between sugarcane genotypes, and their interactions with the environment are important factors to be considered (Pascali *et al.*, 2019; Quandahor *et al.*, 2019; Savi *et al.*, 2019). This may occur due to the rupture of the vascular bundle, which aggravates the damage to plants (Haile, 2000).

This thesis investigates sugarcane's physiological and spectral responses to remote sensing when infested by the sugarcane borer and sugarcane billbug. It is assumed that attacks by *S. levis* and *D. saccharalis* may obstruct the flow of water and nutrients, creating symptoms similar to those caused by water deficit. Boring the stem

or rhizome may possibly alter the sugarcane gas exchange parameters. Therefore, understanding how herbivory influences photosynthetic processes, such as water vapor transfer, respiration, and water use efficiency is fundamental. These processes determine plant growth, development, and fitness, and herbivory can have short- and long-term consequences, especially in synergy with other stressors, such as water deficit. This thesis is divided into four chapters, in which the second chapter addresses the interaction between water stress and sugarcane borer infestation and its impacts on gas exchange and the spectral response of sugarcane. The third chapter depicts a study in sugarcane fields that compares the suitability of multispectral sensors coupled to UAVs and satellites for detection and potential monitoring tools for the sugarcane billbug. The fourth chapter discusses the contributions and limitations of this study regarding current sugarcane pest monitoring tools.

References

ATTRI, I.; AWASTHI, L. K.; SHARMA, T. P. Machine learning in agriculture: a review of crop management applications. **Multimedia Tools and Applications**, v. 83, n. 5, p. 12875–12915, 2024.

BARBEDO, J. G. A. A review on the combination of deep learning techniques with proximal hyperspectral images in agriculture. **Computers and Electronics in Agriculture**, v. 210, p. 107920, 2023.

BEHMANN, J.; MAHLEIN, A. K.; RUMPF, T.; RÖMER, C.; PLÜMER, L. A review of advanced machine learning methods for the detection of biotic stress in precision crop protection. **Precision Agriculture**, v. 16, n. 3, p. 239–260, 2015.

CONAB. **Acompanhamento safra brasileira de cana-de-açúcar - Safra 2023/24, n.4 - Quarto levantamento**. Disponível em: <https://www.conab.gov.br/info-agro/safras/cana>. Acesso em: 14 jul. 2024.

DARA, S. K. The new Integrated Pest Management paradigm for the modern age. **Journal of Integrated Pest Management**, v. 10, n. 1, 2019.

DINARDO-MIRANDA, L. L. Nematóides e pragas de solo em cana-de-açúcar. **Informações agronômicas nº 110**, v. 1, p. 25–32, 2005.

DLAMINI, P. J. Drought stress tolerance mechanisms and breeding effort in sugarcane: a review of progress and constraints in South Africa. **Plant Stress**, v. 2, p. 100027, 2021.

HAILE, F. J. Drought stress, insects, and yield loss. *Em*: PETERSON, R. K. D.; HIGLEY, L. G. (Eds.). **Biotic stress and yield loss**. 1st. ed. Boca Raton, USA: CRC Press, 2000. p. 117–133.

HIGLEY, L.; PEDIGO, L. **Economic thresholds for integrated pest management**. Nebraska, USA: University of Nebraska Press, 1996.

HUSSAIN, H. A.; HUSSAIN, S.; KHALIQ, A.; ASHRAF, U.; ANJUM, S. A.; MEN, S.; WANG, L. Chilling and drought stresses in crop plants: implications, cross talk, and potential management opportunities. **Frontiers in Plant Science**, v. 9, p. 348835, 2018.

INMAN-BAMBER, N. G.; LAKSHMANAN, P.; PARK, S. Sugarcane for water-limited environments: theoretical assessment of suitable traits. **Field Crops Research**, v. 134, p. 95–104, 2012.

JENSEN, J. R. **Remote sensing of the environment: an earth resource perspective**. 2. ed. Upper Saddle River, USA: Pearson Prentice Hall, 2007.

LYNCH, J. P. Edaphic stress interactions: important yet poorly understood drivers of plant production in future climates. **Field Crops Research**, v. 283, p. 108547, 2022.

NANSEN, C. The potential and prospects of proximal remote sensing of arthropod pests. **Pest Management Science**, v. 72, n. 4, p. 653–659, 2016.

NANSEN, C.; ELLIOTT, N. Remote sensing and reflectance profiling in entomology. **Annual Review of Entomology**, v. 61, n. 1, p. 139–158, 2016.

PANDEY, P.; IRULAPPAN, V.; BAGAVATHIANNAN, M. V.; SENTHIL-KUMAR, M. Impact of combined abiotic and biotic stresses on plant growth and avenues for crop improvement by exploiting physio-morphological traits. **Frontiers in Plant Science**, v. 8, p. 237767, 2017.

PASCALI, M. DE *et al.* Molecular effects of *Xylella fastidiosa* and drought combined stress in olive trees. **Plants**, v. 8, n. 11, p. 437, 2019.

PEDIGO, L. P.; HUTCHINS, S. H.; HIGLEY, L. G. Economic Injury Levels in theory and practice. **Annual Review of Entomology**, v. 31, p. 341–368, 1986.

PETERSON, R. K. D.; HIGLEY, L. G.; PEDIGO, L. P. Whatever happened to IPM? **American Entomologist**, v. 64, n. 3, p. 146–150, 2018.

QUANDAHOR, P.; LIN, C.; GOU, Y.; COULTER, J. A.; LIU, C. Leaf morphological and biochemical responses of three Potato (*Solanum tuberosum* L.) cultivars to drought stress and aphid (*Myzus persicae* Sulzer) infestation. **Insects**, v. 10, n. 12, p. 435, 2019.

ROSSATO, J. A. S.; COSTA, G. H. G.; MADALENO, L. L.; MUTTON, M. J. R.; HIGLEY, L. G.; FERNANDES, O. A. Characterization and impact of the sugarcane borer on sugarcane yield and quality. **Agronomy Journal**, v. 105, n. 3, p. 643–648, 2013.

SAVI, T.; GARCÍA GONZÁLEZ, A.; HERRERA, J. C.; FORNECK, A. Gas exchange, biomass and non-structural carbohydrates dynamics in vines under combined drought and biotic stress. **BMC Plant Biology**, v. 19, n. 1, p. 1–11, 2019.

SHAIKH, T. A.; RASOOL, T.; LONE, F. R. Towards leveraging the role of machine learning and artificial intelligence in precision agriculture and smart farming. **Computers and Electronics in Agriculture**, v. 198, p. 107119, 2022.

SHINDE, P. P.; SHAH, S. A review of machine learning and deep learning applications. **Proceedings - 2018 4th International Conference on Computing, Communication Control and Automation, ICCUBEA 2018**, 2018.

TOTH, C.; JÓŹKÓW, G. Remote sensing platforms and sensors: a survey. **ISPRS Journal of Photogrammetry and Remote Sensing**, v. 115, p. 22–36, 2016.

XAVIER, G. G.; SÁ FARIAS, E. DE; CARMO, D. DAS G. DO; GUEDES, A. G.; SAMUELS, R. I.; FREITAS, D. R. DE; PEREIRA, E. J. G.; LIMA, E.; PICANÇO, M. C. Determining factors and economic injury levels for *Sphenophorus levis* for chemical and biological control in irrigated and non-irrigated sugarcane crops. **Neotropical Entomology**, 2024.

ZANDALINAS, S. I.; MITTLER, R. Plant responses to multifactorial stress combination. **New Phytologist**, v. 234, n. 4, p. 1161–1167, 2022.

ZANDALINAS, S. I.; PELÁEZ-VICO, M. Á.; SINHA, R.; PASCUAL, L. S.; MITTLER, R. The impact of multifactorial stress combination on plants, crops, and ecosystems: how should we prepare for what comes next? **The Plant Journal**, v. 117, n. 6, p. 1800–1814, 2024.

ZHANG, J.; HUANG, Y.; PU, R.; GONZALEZ-MORENO, P.; YUAN, L.; WU, K.; HUANG, W. Monitoring plant diseases and pests through remote sensing technology: a review. **Computers and Electronics in Agriculture**, v. 165, p. 104943, 2019.

ZHANG, T.; ZHANG, W.; YANG, R.; LIU, Y.; JAFARI, M. CO2 capture and storage monitoring based on remote sensing techniques: a review. **Journal of Cleaner Production**, v. 281, p. 124409, 2021.

ZUBLER, A. V.; YOON, J. Y. Proximal methods for plant stress detection using optical sensors and machine learning. **Biosensors 2020, Vol. 10, Page 193**, v. 10, n. 12, p. 193, 2020.

CHAPTER 2 – Interaction between water deficit and injury of sugarcane borer (Lepidoptera: Crambidae) in the gas exchange parameters and spectral reflectance of the sugarcane

Resumo

As plantas estão sujeitas a uma diversidade de estressores que eventualmente limitam seu desenvolvimento e produtividade. Entretanto, a análise dos efeitos da combinação entre estresses abióticos e bióticos normalmente é desconsiderada. A combinação entre estresses pode ter efeitos sinérgicos ou antagônicos, e, portanto, necessitam de maior esclarecimento para uma tomada de decisão assertiva. Nesse estudo, examinamos como a interação entre o estresse hídrico e a injúria da broca-da-cana alteram aspectos fisiológicos da cana-de-açúcar através das trocas gasosas. Nossos resultados mostram que ambos os estressores alteram a fisiologia da cana-de-cana, mas não é possível distinguir entre os efeitos da injúria da broca-da-cana e aqueles causados pelo déficit hídrico. Também foi demonstrado que os estresses, isolados ou combinados, interferem nos parâmetros de trocas gasosas independente do período pós infestação e da variedade. Entre os parâmetros que apresentaram diferença para a combinação de estressores estão transpiração (E), condutância estomática (gs) e assimilação de CO_2 (A). A relação entre tamanho da injúria (comprimento da galeria) e os parâmetros de trocas gasosas somente foram significativos para concentração intercelular de CO_2 (Ci) e eficiência de uso da água (WUE). Foi observado uma relação positiva e negativa para Ci e WUE respectivamente. A resposta espectral das plantas de cana-de-açúcar mostrou-se semelhante independentemente dos tratamentos, com baixas métricas de classificação dos modelos de *machine learning*. O conhecimento gerado deste estudo fundamenta a possibilidade de refinamento dos limiares econômicos para a broca-da-cana na cana-de-açúcar, uma vez que alterações na tolerância da cana imposta pela restrição hídrica podem alterar o nível atual aplicado.

Palavras-chave: estressores, interação inseto-planta, tomada de decisão, trocas gasosas.

Abstract

Plants are subject to a variety of stressors that will eventually limit their development and yield. However, analysis of the combination of abiotic and biotic stresses is usually disregarded. The combination of stresses can have synergistic or antagonistic effects and, therefore, they require greater clarification for assertive decision-making. In this study, we examined how the interaction between water stress and sugarcane borer injury alters the physiological aspects of sugarcane through gas exchange parameters and foliar reflectance. Our results show that both stressors alter sugarcane physiology, but it is not possible to distinguish between the effects of sugarcane borer injury and those caused by water deficit. Stresses, whether isolated or combined, disrupt gas exchange parameters, regardless of the post-infestation period and sugarcane variety. Among the differences that make a difference to the combination of stressors are transpiration (E), stomatal conductance (gs), and CO_2 assimilation (A). The relationship between lesion size (gallery length) and gas exchange parameters was significant only for intercellular CO_2 concentration (Ci) and water use efficiency (WUE). A positive and negative relationship was observed for Ci and WUE, respectively. The spectral response of sugarcane plants was similar regardless of treatments, with low classification metrics from machine learning models. The knowledge generated from this study supports the possibility of refining the economic thresholds (EIL) for the sugarcane borer in sugarcane since changes in sugarcane tolerance imposed by water restrictions can alter the current threshold applied.

Keywords: stressors, insect-plant interaction, decision making, gas exchange.

Introduction

Abiotic and biotic stresses are the main limiting factors in plant growth and development. The impact of stressors on plants can vary depending on the severity and duration of stress, development stage, tissue type, and interactions among multiple stresses (Taiz *et al.*, 2015; Ramegowda *et al.*, 2020). For instance, the combination of abiotic and biotic stresses can alter the signaling pathways of plant defense, either activating or suppressing defensive responses (Azevedo *et al.*, 2011; Pascali *et al.*, 2019; Zhong *et al.*, 2024).

The assessment of the impacts of abiotic and biotic stresses on plants has usually been carried out individually, disregarding the effects of their interactions (Pandey *et al.*, 2017; Ramegowda *et al.*, 2020). This is because, in general, dividing and quantifying the effects of multiple stressor interactions in plants are not an easy task. (Haile, 2000; Rossato *et al.*, 2019; Savi *et al.*, 2019). However, agroecosystems often expose plants to simultaneous abiotic and biotic stresses, which can significantly impact their development and yield. Additionally, the genetic differences between genotypes, the effects of abiotic and biotic stressors on plants, and their interaction with the growing environment should all be considered when evaluating the quantitative and qualitative responses of plants to these types of stressors (Porto *et al.*, 2019; Quandahor *et al.*, 2019; Savi *et al.*, 2019).

Despite its rusticity among the cultivated plants, sugarcane (*Saccharum* spp.) is also subject to several stressors that constrain its potential yield. Water restriction, for example, is considered the most limiting abiotic factor stress for sugarcane production (Lakshmanan and Robinson, 2013). Under water restriction, plants conserve water to balance their use and consequently reduce CO_2 capture, carbon fixing, and metabolic processes by closing the stomata *(*Lakshmanan and Robinson, 2013; Ramegowda *et al.*, 2020; Taiz *et al.*, 2015). Stress also changes physiological signaling molecules like trehalose, hydrogen peroxide (H_2O_2), malonic aldehyde (MDA), and the activity of enzymes that detoxify free radicals, including superoxide dismutase (SOD), catalase (CAT), and ascorbate peroxidase (APX) (Azevedo *et al.*, 2011; Siddique *et al.*, 2016; Pascali *et al.*, 2019). These by-products trigger response cascades, modifying metabolic and molecular pathways to defend the plant (Sathyabhama *et al.*, 2015; Zhong *et al.*, 2024).

Many of the physiological and chemical properties of plants influence how their tissues reflect and absorb light (Nilsson, 1995). These properties can change under stress and alter the reflectance spectrum of the leaves (Ennouri and Kallel, 2019). Advances in optical devices, such as hyperspectral sensors, offer greater potential for rapid stress detection by capturing hundreds of individual wavelengths or narrow wavebands of reflected electromagnetic energy from targets (Jensen, 2007). Combined with machine learning tools, this information has accurately classified many instances, both abiotic and biotic stressors in plants (Ennouri and Kallel, 2019; Mahanta *et al.*, 2024; Zhang *et al.*, 2019).

In recent decades, several works have investigated the impact of water deficits on sugarcane genotypes and have provided important insights into the physiological responses of plants when facing this stress are still scarce (Lakshmanan and Robinson, 2013; Pandey *et al.*, 2017). Understanding the mechanisms by which insect-induced herbivory, in combined with other stressors, alters the plant physiology is essential for improving pest monitoring programs, developing prediction models, making informed decisions to mitigate potential losses, and even contributing to genetic breeding programs (Peterson, Higley and Pedigo, 2018).

The sugarcane borer (SB) *Diatraea saccharalis* (Fabricius, 1794) (Lepidoptera: Crambidae). SB is one of the main pests affecting sugarcane (Sandhu and Cherry, 2018). The larvae damage sugarcane by boring holes and galleries in the culms, leading to yield loss and increase plant susceptibility to fungi attack, which cause the red rot disease complex (*Colletotrichum* spp. and *Fusarium* spp.), as well as the death of the buds and physiological disorders in the lateral culm buds (Rossato *et al.*, 2013; Sandhu and Cherry, 2018). Occasionally, SB larvae tunnel circular galleries, weakening the culm and potentially causing plants to fall due to wind action. A SB attack during initial growth when plants have not the internodes developed causes a central leaf yellowing, a symptom known as a “dead heart”. The SB associated with phytopathogenic fungi is responsible for average productivity losses between 0.52 and 1.10% of sugar for every 1% of bored internodes (Rossato *et al.*, 2013).

In this work, we investigated how water stress and SB injury alter the physiological and spectral profiles of sugarcane. It is hypothesized that injury caused by SB larvae triggers a series of morphophysiological responses in sugarcane plants. Due to the characteristic injury caused by the pest, it is assumed that SB injury blocks the passage of water and essential elements to the aerial parts of the plant and

generates symptoms similar to those of a water deficit. However, we believe that these stresses can be distinguished from each other.

Materials and Methods

Plants

Pre-sprouted sugarcane seedlings of the varieties CT 022994 and CTC 4 were multiplied according to Landell *et al.*, (2013) and transferred to plastic pots (22 L capacity) containing 23 kg of agricultural soil from the 0-30 cm profile to maintain the porous space and water capacity retention. The plants were kept in a greenhouse at 27 ± 3 °C, RH 70 ± 10%, and natural light. An automatic irrigation system supplied daily water to the plants until the start of the experiment, 120 days after transplantation (DAT) of seedlings. To standardize the number of culms per pot, we removed less developed culms during the tillering phase (approximately at 50 DAT), ensuring that each pot had only one culm remaining.

Experimental design

The experiment followed a randomized block design in the factorial scheme 2x2x2 (**Table 1**), i.e., two water regimes (NS = no water deficit; WS = water deficit), two infestation levels (C = control – no infestation; DS = SB infested), and two sugarcane varieties (CTC 4 and CT 022994) (Braga Junior *et al.*, 2023). The selection of the varieties represents common cultivars in the state of São Paulo, Brazil, and intrinsic differences to the water regime, where the variety CT 022994 is considered drought-tolerant, and the CTC 4 would represent a susceptible standard.

Each treatment had twenty pots, each of which was considered a replication and contained a single sugarcane plant, totaling 160 pots. To simulate water deficit, plants were subjected to a water regime of either 60% or 100% of soil water retention capacity (WRC), representing deficit and non-deficit conditions, respectively. The water deficit was controlled by daily weighing of the pots, and water was replenished based on the average weight loss of 12 pots per treatment regardless of the variety.

Table 1. Factorial experiment setting, where two sugarcane varieties were subjected to two irrigation regimes (no water stress [NS] vs. water restriction [WS]) and the attack by sugarcane borer (no SB infestation [C] vs. SB infested)

Treatment	Variety	Water regime	Infestation
NSC	CT 022994	100% WRC	Control
NSDS	CT 022994	100% WRC	Infested
NSC	CTC 4	100% WRC	Control
NSDS	CTC 4	100% WRC	Infested
WSC	CT 022994	60% WRC	Control
WSDS	CT 022994	60% WRC	Infested
WSC	CTC 4	60% WRC	Control
WSDS	CTC 4	60% WRC	Infested

The artificial infestation of SB larvae occurred only when the pots from the water deficit treatments (WSC and WSDS) reached a mass corresponding to the soil water content of 60% WRC. Third instar SB larvae (15 days after emergence of the larvae), supplied by a biofactory of biological control agents, were transferred and positioned with the help of a brush of thin hair close to the sheath of +2 and +3 leaves of the plants (**Figure 1 A**). We examined the insects for 48 hours to confirm they had entered into the culm. The survey was based on the observation of the presence of an input hole in the culm (**Figure 1 B**), and plants were reinfested when necessary.

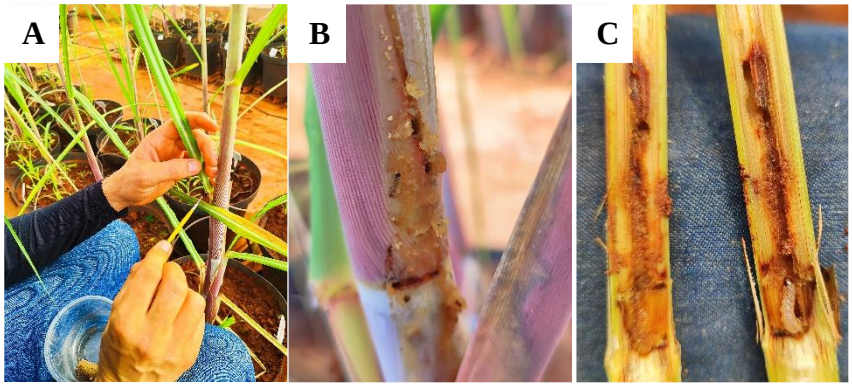


Figure 1 – Details of the artificial sugarcane borer (SB) infestation: (A) artificial infestation of third instar larvae in plants; (B) preliminary inspection of infestations; (C) final inspection to establish the infestation success.

Gas exchange measurements

Initial gas exchange parameters were collected 72 h after the SB artificial infestation of larvae and repeated the process every five days, resulting in four samplings, i.e., 3-, 8-, 13- and 18-days post infestation (DPI). This allowed for analysis

during the larval development period of *D. saccharalis* (Tomaz *et al.*, 2018). In the first evaluation, we randomly selected six pots (reps) of each treatment from the twenty available and kept them until the end of the experiment. The readings were performed with the IRGA CIRAS-3 (PP Systems®, Amesbury, MA, USA) between 9:00 am and 11:30 am. The reference CO_2 concentration and light intensity within the foliar chamber were kept constant at 400 µmol CO_2 mol^{-1} and light intensity set to 1500 µmol m^{-2} s^{-1}, respectively. The collection of information consisted of 3 readings (replicas) at an interval of 10 s in each pot (sampling unit), taken on the +1 leaf (first newly developed leaf, showing the visible auricle), in the median portion. The following parameters were measured: intercellular concentration of CO_2 (Ci) (µmol CO_2 mol^{-1}), stomatal conductivity (gs) (mmol H_2O m^{-2} s), transpiration (E) (mmol H_2O m^{-2} s^{-1}), vapor pressure deficit leaf-air (VPD) (kPa), photosynthetic water use efficiency (WUE) (mmol CO_2 mol^{-1} H_2O), and assimilation/respiration (A) (µmol CO_2 m^{-2} s^{-1}).

Foliar spectral measurements

A hyperspectral sensor captured the reflectance readings of sugarcane plants subjected to both stresses. The measuring instrument was a portable ASD FieldSpec spectroradiometer, HandHeld UV/VNIR® model, operating in the spectral range between 375 and 1075 nm, configured in 512 channels with a 1.6 nm spectrum resolution (ASD, 2002). The measurements were carried out at night to ensure uniformity of lighting. The auxiliary artificial lighting consisted of 2 reflectors carrying 500 W power halogen lamps (Ourolux®, São Paulo, Brazil) positioned at a 30° angle towards the target (Vohland *et al.*, 2011). The lamps were turned on 15 minutes before the readings to stabilize the temperature deviation and ensure the uniformity of the lighting.

Hyperspectral samples were recorded of the twenty pots by treatment and sugarcane variety directly from the nadir position, with the sensor positioned on a tripod at an approximate height of 20 cm above the +1 leaf of the plants, with restriction of the sensor's target field to 1°. For each sample element, the average of five repetitions of the target radiance reading and the radiance of a reference lambertian surface (a Spectralon® plate) were used in the same lighting and observation conditions to estimate the target’s reflectance factor. After the readings, the information was

extracted in the Viewspec Pro v 6.2 software (ASD, 2002) to obtain the reflected radiance. We then calculated the reflectance using the following equation:

$$Reflectance = \frac{R_{target}}{R_{reference}} \times K$$

in which: R_{target} is the radiance reflected by the target, $R_{reference}$ is the radiance reflects by the spectralon plate and K is the correction factor of the plate.

We converted the radiance values to reflectance, and then used the average of the five readings per pot to create a single curve per sample element. A 5-point Savitzky-Golay filter was then applied to smooth the curves in order to minimize the effect of noises caused by external interference to the target and by the inaccuracies of the instrument (Savitzky and Golay, 1964). Readings with values ± 5 standard deviations from the overall average were considered “outliers” and discarded from subsequent processing.

Estimate of the sugarcane borer injury extent impacts on gas exchange traits

At the end of the experiment, all plants were carefully inspected for undue infestations in control plants (no infestation) and the success of infesting in plants intended for this treatment (**Figure 1 C**). Non-infested plants were relocated to the control treatment corresponding to the submitted water regime, i.e., uninfected plants from the NSDS treatment were transferred to the NSC. During the inspection of the culms, the length of the SB galleries was also measured to determine the extent of the injury in the sugarcane culms with the help of a measurement tape.

Data analysis

As the experimental design involved repeated measurements, mixed linear models were adjusted to simultaneously assess the combined effects of the sugarcane borer and water regime, sugarcane variety, and day post-SB infestation - DPI - (fixed effects). The pots (sample units) were considered as a random effect for each of the physiological parameters raised by IRGA. Initially, cases of significant interaction were investigated, comparing the significance of models with interactive and additive factors through a likelihood ratio test. Then the normality and homogeneity of the residuals

were inspected. To determine which group averages were significantly different, gas parameters that had significant effects were subjected to contrast with the p value adjusted by the Bejamini-Hockberg method (Benjamini and Hochberg, 1995; Waite and Campbell, 2006). Further regression models were adjusted considering the data collected at 18 DPI as dependent variables and the length of the SB larvae gallery to verify the influence of the injury size and gas exchange parameters.

For the sugarcane foliar reflectance dataset, machine learning classification models were used to categorize the combination of stress classes. The exercise consisted of classifying each sampling date separately, as well as the whole dataset (**Table 2**). Modeling was initially implemented by dividing the data randomly for training and testing, considering an 80:20 ratio, respectively. The training data was further subdivided into smaller sets to estimate the test error associated with a given model (model evaluation) and select the appropriate model's hyperparameters. The resampling method was k-fold cross-validation. In our study, the training data were divided into five equal parts and repeated three times.

Table 2. Performance of the algorithms tested in the training data. The winning data set and algorithm is highlighted in bold

Dataset	Algorithm	Balanced accuracy	F1-score	Precision	Recall
3 DPI	Multinomial regression	0.55 ± 0.01	0.32 ± 0.01	0.32 ± 0.01	0.32 ± 0.01
	Random Forest	0.57 ± 0.0	0.32 ± 0.03	0.30 ± 0.03	0.32 ± 0.03
	XGBoost	0.56 ± 0.01	0.31 ± 0.02	0.31 ± 0.02	0.34 ± 0.02
	SPLS-DA	0.51 ± 0.02	0.26 ± 0.02	0.29 ± 0.02	0.27 ± 0.03
8 DPI	Multinomial regression	0.57 ± 0.01	0.32 ± 0.02	0.33 ± 0.03	0.35 ± 0.02
	Random Forest	0.53 ± 0.01	0.27 ± 0.02	0.32 ± 0.03	0.29 ± 0.02
	XGBoost	0.50 ± 0.00	0.45 ± 0.03	0.30 ± 0.02	0.25 ± 0.00
	SPLS-DA	0.52 ± 0.01	0.26 ± 0.02	0.30 ± 0.03	0.29 ± 0.02
13 DPI	**Multinomial regression**	**0.64 ± 0.02**	**0.44 ± 0.02**	**0.48 ± 0.03**	**0.46 ± 0.02**
	Random Forest	0.63 ± 0.02	0.43 ± 0.02	0.45 ± 0.02	0.45 ± 0.02
	XGBoost	0.63 ± 0.02	0.43 ± 0.03	0.45 ± 0.03	0.44 ± 0.03
	SPLS-DA	0.64 ± 0.02	0.42 ± 0.03	0.45 ± 0.04	0.45 ± 0.03
18 DPI	Multinomial regression	0.57 ± 0.02	0.32 ± 0.02	0.35 ± 0.03	0.35 ± 0.02
	Random Forest	0.55 ± 0.01	0.29 ± 0.01	0.33 ± 0.02	0.33 ± 0.02
	XGBoost	0.54 ± 0.01	0.28 ± 0.02	0.31 ± 0.03	0.31 ± 0.02
	SPLS-DA	0.57 ± 0.02	0.33 ± 0.03	0.33 ± 0.03	0.36 ± 0.02
All DPI	Multinomial regression	0.55 ± 0.01	0.32 ± 0.01	0.32 ± 0.01	0.32 ± 0.01
	Random Forest	0.58 ± 0.01	0.35 ± 0.01	0.36 ± 0.01	0.36 ± 0.01
	XGBoost	0.56 ± 0.01	0.33 ± 0.01	0.34 ± 0.01	0.34 ± 0.01
	SPLS-DA	0.53 ± 0.01	0.26 ± 0.01	0.31 ± 0.02	0.29 ± 0.01

*DPI: Days after infestation

Four algorithms were tested to determine the one with the best accuracy and precision of the stressor classes. Among the algorithms selected are random decision trees (“Random Forest”), extreme gradient boosting trees (XGBoost), multinomial lasso regression, and sparse partial least squares regression for discriminatory analysis (“SPLS-DA”) (Chun and Keleş, 2010; Belgiu and Drăgu, 2016; Chen and Guestrin, 2016; Nibbering and Hastie, 2022). The models were trained and compared to each other to find out which had the best classification accuracy using the metrics balanced accuracy, F1-score, precision, and recall for all the subsets of data (**Table**

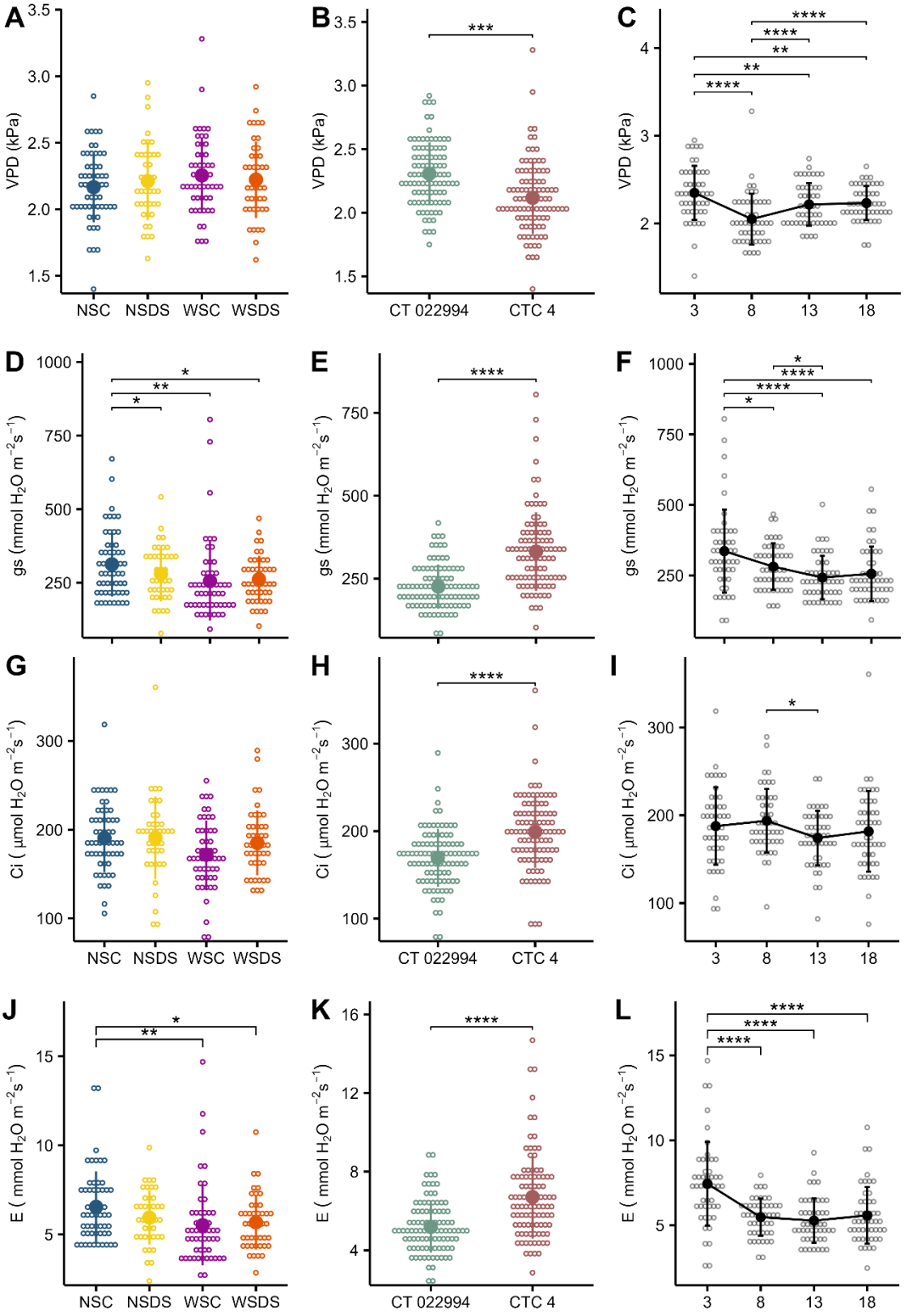
2). The algorithm that conferred the best metrics in the training dataset was evaluated in the test data, with the subsequent construction of a confusion matrix.

The analyses were carried out with the packages “tidyverse” (Kuhn and Wickham, 2020), “lme4” (Bates *et al.*, 2015), “LmerTest” (Kuznetsova, Brockhoff and Christensen, 2017), “DHARMa” (Hartig, 2022), “rstatix” (Kassambara, 2023a), and the graphs were plotted through the “ggpubr” package (Kassambara, 2023b). Classification models were implemented using the “Tidymodels” package (Kuhn and Wickham, 2020). All analyses were done in R software version 4.3.1 (R Core Team., 2023).

Results

Influence of the combination of stressors on sugarcane gas exchange parameters

The parameters evaluated showed no significant interaction between sugarcane varieties, treatments (water stress and sugarcane borer infestation), and days after infestation (DPI) (**Supplementary Table 1**). As a result, the simple effects of the factors studied were considered. The effects of the stressors did not significantly affect the vapor pressure deficit – VPD ($F_{3, 43} = 0.73$; $p = 0.54$; $\eta_p^2 = 0.05$) (**Figure 2 A**), intercellular concentration of CO_2 (Ci) ($F_{3, 43} = 0.12$; $p = 0.12$; $\eta_p^2 = 0.12$) (**Figure 2 G**), and water use efficiency – WUE ($F_{3, 43} = 0.25$; $p = 0.25$; $\eta_p^2 = 0.09$) (**Figure 2 P**) in sugarcane leaves (**Supplementary Table 3**). Meanwhile, significant changes were observed in the effects of stressors for E parameters ($F_{3,43} = 5.08$; $p = 0.00042$; $\eta_p^2 = 0.26$), gs ($F_{3,43} = 5.70$; $p = 0.0022$; $\eta_p^2 = 0.28$) and A ($F_{3,43} = 3.12$; $p = 0.036$; $\eta_p^2 = 0.18$). The contrasts point out differences primarily between plants not subject to stressors (NSC) and plants in combination with any of the abiotic or biotic stressors (NSDS, WSC, and WSDS) (**Figure 2 D**, **J**, **M**). There was a significant reduction between these parameters with the estimated mean values of 0.17 mmol H_2O m^{-2} s^{-1}, 58.6 mmol M^{-2} s^{-1}, and 3.58 µmol CO_2 m^{-2} s^{-1} for E, gs, and A (**Supplementary Table 2**).


A
B
C
D
E
F
G
H
I
J
K
L
VPD (kPa)
gs (mmol H2O m-2s-1)
Ci (µmol H2O m-2s-1)
E (mmol H2O m-2s-1)
NSC
NSDS
WSC
WSDS
CT 022994
CTC 4
3
8
13
18

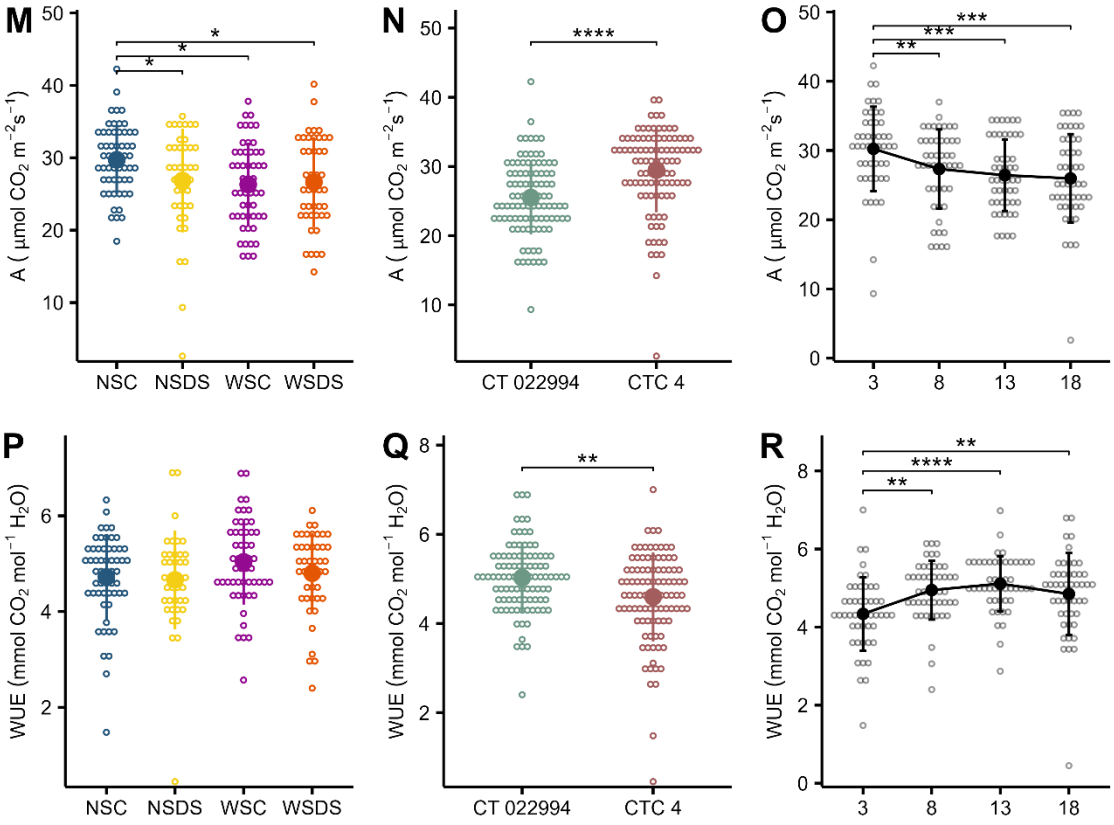


Figure 2 – Vapor pressure deficit (VPD) (A-C), stomata conductivity (gs) (D-E), Intercellular concentration of CO_2 (Ci) (G-I), transpiration (E) (J-L), CO_2 assimilation (liquid photosynthesis) (A) (M-O) and water use efficiency (WUE) (P-R) of plants subjected to the combination of abiotic and biotic stressors (NSC: no water restriction and no sugarcane borer infestation; NSDS: no water restriction with sugarcane borer infestation; WSC: water restriction and no sugarcane borer infestation; WSDS: water restriction with sugarcane borer infestation); (A, D, G, J, M, P), sugarcane varieties (CT 022994 and CTC 4) (B, E, H, K, N, Q), and different post-infestation periods (DPI) (3, 8, 13, and 18 days after infesting) (C, F, I, L, O, R). Full circles with vertical bars and open circles represent the average value ± standard deviation (SD) and raw data, respectively. Brackets delimit the significant contrasts. *p < 0.05; **p < 0.01; ***p < 0.001; ****p < 0.0001.

Differences were observed between the varieties and DPI, regardless of the physiological parameter raised (**Supplementary Table 3**). The CTC 4 variety demonstrated higher values among the gas parameters (gs: $F_{1,43} = 57.97$; $p < 0.0001$; $\eta_p^2 = 0.57$; Ci: $F_{1,43} = 22.56$; $p < 0.0001$; $\eta_p^2 = 0.34$; E: $F_{1,43} = 36.62$; $p < 0.0001$; $\eta_p^2 = 0.46$; A: $F_{1,43} = 17.85$; $p = 0.00012$; $\eta_p^2 = 0.29$), except VPD and WUE (VPD: $F_{1,43} = 17.85$; p

= 0.00012; η_p^2 = 0.29; WUE: $F_{1,43}$ = 10.04; p = 0.0028; η_p^2 = 0.19) (**Figure 2 B, E, H, K, N, Q**). Average increases of 16.34% were observed in Ci, 12.82% in E, 6.68% in gs, and 13.94% in A, and a decrease of 7.95% and 9.48% in VPD and WUE in variety CTC 4 compared to CT 022994 (**Supplementary Table 2**).

The relationship between gallery length and gas exchange response was only significant for Ci and WUE (**Figure 3**). For these parameters, there is a twice increase for Ci and decrease of 0.047 per centimeter of length of injured tissue by SB larvae for WUE (**Figure 3 C** and **F**).

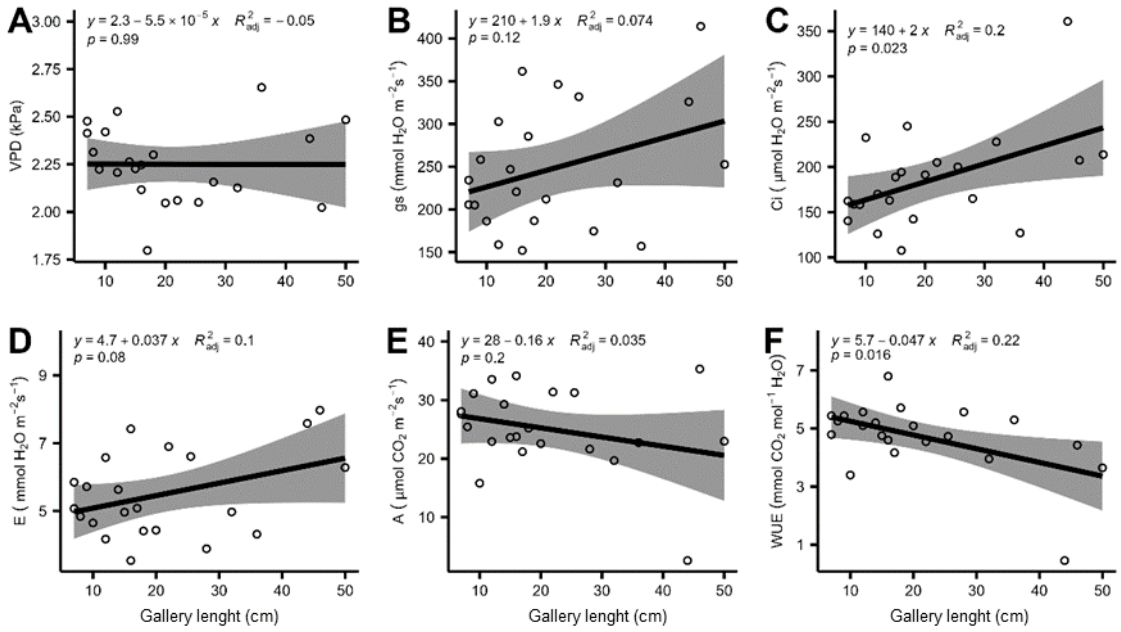


Figure 3 – Relation between the size of the injury of the sugarcane borer (SB) on sugarcane gas exchange parameters. The shaded area represents the confidence interval (95%).

Water regime and sugarcane borer combination on sugarcane spectral reflectance

Among the algorithms tested, multinominal regression performed the best over the others. However, their ability to correctly classify treatments was poor, with balanced accuracy values below 0.7 regardless of post-infestation date (DPI) or complete dataset (**Table 2**). The 13 DPI data set, which presented the best performance with values above 0.60 for balanced accuracy and F1-score, precision, and recall above 0.4 (**Table 2**).

From the 13 DPI dataset, the multinominal regression obtained a balanced accuracy of 0.72 in the test data (**Table 3**). The confusion matrix shows that there were problems when separating classes referring to treatments that share the same water regime (**Table 3**).

Table 3. Metrics and confusion matrix of the winning algorithm at 13 DPI

Dataset	Algorithm	Balanced accuracy	F1-score	Precision	Recall
13 DPI*	Multinomial regression	0.72	0.57	0.58	0.58

Penalization: $1.51\ 10^{-10}$

Confusion Matrix

		Observed			
		NSC	NSDS	WSC	WSDS
Predicted	NSC**	8	1	1	1
	NSDS	2	3	0	1
	WSC	1	1	4	2
	WSDS	0	1	2	4

*DPI: Days after infestation

**NSC: No water stressed, no SB infestation; NSDS: no water stressed, SB infested; WSC: water stressed, no SB infestation; WSDS: water stressed, SB infested.

Discussion

In our study model, we sought to investigate the relationship between injury caused by the sugarcane borer, a culm boring phytophagous insect, and controlled water stress (60% WRC), isolated or combined, to the gas exchange parameters of the leaves in two sugarcane varieties. Our assumption was that the sugarcane borer larvae attack could interfere with the transport of water and nutrients by destroying the culm conductive vessels. Such an effect could mimic symptoms similar to water deficiency, but it would be possible to differentiate sugarcane plant responses between the two stressors. In fact, it has been revealed that there is an interference of the sugarcane borer attack in the physiology of the sugarcane, although it has not been possible to differentiate its effects from those promoted by the established water stress level. We showed that both stresses, isolated or combined, interfere with some of the gas exchange and spectral reflectance parameters evaluated, regardless of the post-introduction period of stress and sugarcane variety. Furthermore, the responses between the varieties differ from one another.

The parameters with significant differences due to stressors were E, gs, and A. These results agree with several other studies on the physiological response of plants to water deficits (Godfrey, Holtzer and Norman, 1991; Pascali *et al.*, 2019; Quandahor et al., 2019; Heimoana *et al.*, 2022). Stomatal closure, or reduced stomatal conductivity, typically accompanies the reduction of liquid photosynthesis. This, in turn, restricts CO_2 entry into the stomata, resulting in a reduced transpiratory coefficient in drier conditions (Azevedo *et al.*, 2011; Taiz *et al.*, 2015; Siddique *et al.*, 2016).

However, studies revealing the effects of phytophagous insect attacks on the physiology of cultivated plants may vary (Welter, 1989; Retuerto *et al.*, 2004). Several reports highlight no significant effect on the photosynthesis rate, stomatal conductivity, CO_2 intercellular concentration, and evaporation, especially in periods close to the introduction of the stressor (Welter, 1989; Retuerto *et al.*, 2004; Savi *et al.*, 2019; Heimoana *et al.*, 2022). In our case, the reduction of E, gs, and A parameters was detected 72 h after plant infestation and remained so throughout the evaluation period, compared with plants that did not experience any kind of stress. Our findings suggest that the effects of herbivory induced by *D. sacharalis* larvae appear to be similar to the stablished water stress level. Results of a field study also showed negative impacts between photosynthetic rates of uninfested plants and plants infested with sugarcane borer, especially in the drier seasons of the year (Rossato *et al.*, 2019). However, further in-depth research is needed to verify whether such responses would not alter in plants subjected to more pronounced water stress levels and the injury imposed by sugarcane borer larvae.

The spectral response of the cane plants was similar among the treatments, since classification metrics were low regardless of the period analyzed. The confusion matrix emphasizes that incorrect classifications primarily involved treatments with similar water regimes, suggesting that the imposed water stress had a more significant impact on the sugarcane's spectral reflectance than SB. In this way, detecting SB attacks through remote sensing may be challenging. Such adversities are intensified in field conditions since in the sugarcane agroecosystem, there are other stress agents that interact with sugarcane and their effects are similar to each other (Yuan *et al.*, 2017; Zhang *et al.*, 2019). Rationally, the use of remote sensing with the objective of monitoring may not be ideal for SB, as the plant would change its spectral profile after larvae bore into the culm. Consequently, the detection of the SB would occur after the

damage occurred and at a time of difficult control since the larvae would be protected inside the culm (Li *et al.*, 2024).

When considering the same injury guild, our results show similar effects to those found by the attack of the European corn borer, *Ostrinia nubilalis* (Hubner 1796) (Lepidoptera: Pyralidae), on the corn physiology (Godfrey, Holtzer and Norman, 1991). The attack of European corn borer had similarities with the effects of water stress on the plant (through a reduction in A, gs, and Ci and an increase in leaf temperature), as observed by Godfrey, Holtzer and Norman, (1991). Similarly, another culm borer, the wheat stem sawfly *Cephus cinctus* Norton, 1872, reduced the liquid photosynthesis of wheat plants regardless of the established water regime (Macedo, Weaver and Peterson, 2007). But, unlike corn and wheat, sugarcane infestations with *D. saccharalis* are associated with fungal infections from *Colletotrichum* spp. and *Fusarium* spp., causing red rot symptoms (Sathyabhama *et al.*, 2015). This symptom is associated with the biochemical defenses of plants through the production of phenols to combat such etiological agents (Ogunwolu *et al.*, 1991; Sathyabhama *et al.*, 2015). As a result, the presence of these fungi can have a negative impact on sugarcane's physiology. However, separating and quantifying its effects from those caused by the sugarcane borer is a difficult task since the fungi is always found associated with insect injury (Franco *et al.*, 2022).

The difference in response between varieties in all parameters was an expected result since they were different genotypes. Interestingly, the variety CT 022994, recognized for its water stress tolerance (CTC, 2024), showed lower values of the gas parameters, except for VPD and WUE. The possible explanations for this answer are not clear. This observation may be associated with differences in the developmental cycle and environmental production requirements among varieties. As recommended by the Centro de Tecnologia Canavieira, the CTC 4 variety has a medium cycle and can be allocated in more restrictive environments (CTC, 2024). In contrast, the variety CT 022994 has a late cycle and is recommended for more productive locations. In an ecological context, the CTC 4 variety would have less time for its development and, consequently, its ripening. Therefore, this genotype would need to produce and accumulate more photoassimilates to compensate for the time lag to maturity, contrary to CT 022994.

When considering the extent of the SB injury in the expression of stress in sugarcane plants, it was intuitively expected that there would be a positive relationship

between the length of the gallery inflicted by larvae and the plant's response to stress. However, no such hypothesis has been proved, which has also not been confirmed in studies on the injury of *D. saccharalis* in rice culture (Lv, Wilson and Longnecker, 2008). Apparently, SB does not destroy all the conductive vessels of the culm, and there is possibly a tolerance or compensation mechanism of the plant. In rice, compensation occurs by issuing new tillers to plants injured in the stem or by increasing the size of the panicles when the injury is observed in the leaves and leaf sheath (Lv, Wilson and Longnecker, 2008). In our case, there are indications for the assumption of compensation, as it was observed that Ci and WUE had significant relationships with the size of the injury; that is, in some way, the plant would increase its internal concentration of CO_2 and would lose more water to keep a level of net photosynthesis that would compensate for the stress imposed. This finding would have relevant ecological significance because if the insect severely affects its host, potentially leading to its death, it could compromise its own development. Conversely, corn plants infested with SB showed contradictory results to those found in this study, in which higher WUE and lower E were observed. (Castro, 2023). Although the three crops share the same family (Poaceae), corn does not have tillering ability like rice and sugarcane, and it is the crop that has undergone the greatest selection pressure through genetic breeding. Consequently, corn may have lost characteristics that confer tolerance to stressors (Marone *et al.*, 2021). Furthermore, our findings indicate that the losses generated by sugarcane borer injury are, for the most part, due to the infection by the fungi of the red rot complex. This would reshape the importance of the pest being a disease vector rather than its direct damage (Franco *et al.*, 2022).

Understanding how the sugarcane tolerates damage from the SB and other stressors is crucial to improve the economic thresholds for managing this pest. If changes are observed in the sugarcane tolerance imposed by environmental conditions, such levels can be changed. Conversely, if sugarcane tolerance can be improved by environmental conditions, there may be no need for control. In this sense, our work brings evidence that the moderate water stress does not alter the sugarcane tolerance to the damage caused by SB, since plants attacked by the pest had a reduction in liquid photosynthesis similar to plants subjected to both stresses and water deficit alone.

References

ASD. **FieldSpec® UV/VNIR: HandHeld Spectroradiometer - User's Guide.** Boulder, USA, 2002.

AZEVEDO, R. A.; CARVALHO, R. F.; CIA, M. C.; GRATÃO, P. L. Sugarcane under pressure: an overview of biochemical and physiological studies of abiotic stress. **Tropical Plant Biology**, v. 4, n. 1, p. 42–51, 2011.

BATES, D.; MÄCHLER, M.; BOLKER, B.; WALKER, S. Fitting linear mixed-effects models using lme4. **Journal of Statistical Software**, v. 67, n. 1, 2015.

BELGIU, M.; DRĂGU, L. Random forest in remote sensing: a review of applications and future directions. **ISPRS Journal of Photogrammetry and Remote Sensing**, v. 114, p. 24–31, 2016.

BENJAMINI, Y.; HOCHBERG, Y. Controlling the false discovery rate: a practical and powerful approach to multiple testing. **Journal of the Royal Statistical Society. Series B (Methodological)**, v. 57, n. 1, p. 289–300, 1995.

BRAGA JUNIOR, R. L. C.; LANDELL, M. G. DE A.; XAVIER, M. A.; KANTHACK, R. A. D.; SILVA, D. N.; BIDÓIA, M. A. P.; SILVA, T. N.; SILVA, V. H. P.; RODRIGUES, P. E.; CARREGARI, H. R.; ANJOS, I. A. **Censo varietal IAC de cana-de-açúcar no Brasil - Safra 2022/23**. Disponível em: <https://www.iac.sp.gov.br/media/publicacoes/iacbt235.pdf>. Acesso em: 4 ago. 2024.

CASTRO, M. G. B. DE. **Respostas fisiológicas e espectrais de plantas de milho infestadas por *Diatraea saccharalis* (Fabricius, 1794) (Lepidoptera: Crambidae) e *Spodoptera frugiperda* (J. E. Smith, 1797) (Lepidoptera: Noctuidae)**. 41 f: Dissertação (Mestrado em Agronomia - Entomologia Agrícola), Unesp - Jaboticabal, 2023.

CHEN, T.; GUESTRIN, C. XGBoost: a scalable tree boosting system. **Proceedings of the ACM SIGKDD International Conference on Knowledge Discovery and Data Mining**, p. 785–794, 2016.

CHUN, H.; KELEŞ, S. Sparse partial least squares regression for simultaneous dimension reduction and variable selection. **Journal of the Royal Statistical Society Series B: Statistical Methodology**, v. 72, n. 1, p. 3–25, 2010.

CTC. **Variedades CTC**. Disponível em: <https://ctc.com.br/produtos/>. Acesso em: 23 jan. 2024.

ENNOURI, K.; KALLEL, A. Remote Sensing: An Advanced Technique for Crop Condition Assessment. **Mathematical Problems in Engineering**, v. 2019, p. 1–8, 17 jul. 2019.

FRANCO, F. P.; TÚLER, A. C.; GALLAN, D. Z.; GONÇALVES, F. G.; FAVARIS, A. P.; PEÑAFLOR, M. F. G. V.; LEAL, W. S.; MOURA, D. S.; BENTO, J. M. S.; SILVA-FILHO, M. C. *Colletotrichum falcatum* modulates the olfactory behavior of the sugarcane borer, favoring pathogen infection. **FEMS Microbiology Ecology**, v. 98, n. 4, p. 1–8, 2022.

GODFREY, L. D.; HOLTZER, T. O.; NORMAN, J. M. Effects of european corn borer (Lepidoptera: Pyralidae) tunneling and drought stress on field corn gas exchange parameters. **Journal of Economic Entomology**, v. 84, n. 4, p. 1370–1380, 1991.

HAILE, F. J. Drought stress, insects, and yield loss. *Em*: PETERSON, R. K. D.; HIGLEY, L. G. (Eds.). **Biotic stress and yield loss**. 1st. ed. Boca Raton, USA: CRC Press, 2000. p. 117–133.

HARTIG, F. **DHARMa: Residual Diagnostics for hierarchical (multi-level / mixed) regression models**, 2022. Disponível em: <https://CRAN.R-project.org/package=DHARMa>

HEIMOANA, S. C.; WILSON, L. J.; CONSTABLE, G. A.; GEORGE, D. L. Do phloem feeders affect gas exchange? A case study of *Aphis gossypii* (Glover) on cotton. **Crop Science**, v. 63, n. 2, p. 912–920, 2022.

JENSEN, J. R. **Remote sensing of the environment: an earth resource perspective**. 2. ed. Upper Saddle River, USA: Pearson Prentice Hall, 2007.

KASSAMBARA, A. **rstatix: pipe-friendly framework for basic statistical tests**, 2023a. Disponível em: <https://cran.r-project.org/package=rstatix>

KASSAMBARA, A. **ggpubr: "ggplot2" based publication ready plots**, 2023b. Disponível em: <https://cran.r-project.org/package=ggpubr>

KUHN, M.; WICKHAM, H. **Tidymodels: a collection of packages for modeling and machine learning using tidyverse principles.**, 2020. Disponível em: <https://www.tidymodels.org>. Acesso em: 15 maio. 2024

KUZNETSOVA, A.; BROCKHOFF, P. B.; CHRISTENSEN, R. H. B. lmerTest package: tests in linear mixed effects models. **Journal of Statistical Software**, v. 82, n. 13, 2017.

LAKSHMANAN, P.; ROBINSON, N. Stress physiology: abiotic stresses. **Sugarcane: Physiology, Biochemistry, and Functional Biology**, p. 411–434, 2013.

LANDELL, M. G. A.; CAMPANA, M. P.; FIGUEIREDO, P.; XAVIER, M. A.; ANJOS, I. A. Sistema de multiplicação de cana-de-açúcar com uso de mudas pré-brotadas (MPB), oriundas de gemas individualizadas. p. 1–16, 2013.

LI, A. M.; CHEN, Z. L.; LIAO, F.; ZHAO, Y.; QIN, C. X.; WANG, M.; PAN, Y. Q.; WEI, S. L.; HUANG, D. L. Sugarcane borers: species, distribution, damage and management options. **Journal of Pest Science 2024**, p. 1–31, 2024.

LV, J.; WILSON, L. T.; LONGNECKER, M. T. Tolerance and compensatory response of rice to sugarcane borer (Lepidoptera: Crambidae) injury. **Environmental Entomology**, v. 37, n. 3, p. 796–807, 2008.

MACEDO, T. B.; WEAVER, D. K.; PETERSON, R. K. D. Photosynthesis in wheat at the grain filling stage is altered by larval wheat stem sawfly (Hymenoptera: Cephidae) injury and reduced water availability. **Journal of Entomological Science**, v. 42, n. 2, p. 228–238, 2007.

MAHANTA, D. K.; BHOI, T. K.; KOMAL, J.; SAMAL, I.; MASTINU, A. Spatial, spectral and temporal insights: harnessing high-resolution satellite remote sensing and artificial intelligence for early monitoring of wood boring pests in forests. **Plant Stress**, v. 11, p. 100381, 2024.

MARONE, D.; RUSSO, M. A.; MORES, A.; FICCO, D. B. M.; LAIDÒ, G.; MASTRANGELO, A. M.; BORRELLI, G. M. Importance of landraces in cereal breeding for stress tolerance. **Plants**, p. 1267, 22 jun. 2021.

NIBBERING, D.; HASTIE, T. J. Multiclass-penalized logistic regression. **Computational Statistics & Data Analysis**, v. 169, p. 107414, 2022.

NILSSON, H. Remote sensing and image analysis in plant pathology. **Annual Review of Phytopathology**, v. 33, n. 1, p. 489–528, 28 set. 1995.

OGUNWOLU, E. O.; REAGAN, T. E.; FLYNN, J. L.; HENSLEY, S. D. Effects of *Diatraea saccharalis* (F.) (Lepidoptera: Pyralidae) damage and stalk rot fungi on sugarcane yield in Louisiana. **Crop Protection**, p. 57–61, 1 fev. 1991.

PANDEY, P.; IRULAPPAN, V.; BAGAVATHIANNAN, M. V.; SENTHIL-KUMAR, M. Impact of combined abiotic and biotic stresses on plant growth and avenues for crop improvement by exploiting physio-morphological traits. **Frontiers in Plant Science**, v. 8, p. 237767, 2017.

PASCALI, M. DE *et al.* Molecular effects of *Xylella fastidiosa* and drought combined stress in olive trees. **Plants**, v. 8, n. 11, p. 437, 2019.

PETERSON, R. K. D.; HIGLEY, L. G.; PEDIGO, L. P. Whatever happened to IPM? **American Entomologist**, v. 64, n. 3, p. 146–150, 2018.

PORTO, N. DE A.; ROQUE, J. V.; WARTHA, C. A.; CARDOSO, W.; PETERNELLI, L. A.; BARBOSA, M. H. P.; TEÓFILO, R. F. Early prediction of sugarcane genotypes susceptible and resistant to *Diatraea saccharalis* using spectroscopies and classification techniques. **Spectrochimica Acta Part A: Molecular and Biomolecular Spectroscopy**, v. 218, p. 69–75, 2019.

QUANDAHOR, P.; LIN, C.; GOU, Y.; COULTER, J. A.; LIU, C. Leaf morphological and biochemical responses of three Potato (*Solanum tuberosum* L.) cultivars to drought stress and aphid (*Myzus persicae* Sulzer) infestation. **Insects**, v. 10, n. 12, p. 435, 2019.

R CORE TEAM. **R: a language and environment for statistical computing.** Disponível em: <https://www.r-project.org/>. Acesso em: 15 jan. 2024.

RAMEGOWDA, V.; COSTA, M. V. J. DA; HARIHAR, S.; KARABA, N. N.; SREEMAN, S. M. Abiotic and biotic stress interactions in plants: a cross-tolerance perspective. *Em*: HOSSAIN, M. A.; LIU, F.; BURRITT, D. J.; FUJITA, M.; HUANG, B. (Eds.). . **Priming-Mediated Stress and Cross-Stress Tolerance in Crop Plants**. London, UK: Academic Press, 2020. p. 267–302.

RETUERTO, R.; FERNANEZ-LEMA, B.; ROILOA, R.; OBESO, J. R. Increased photosynthetic performance in holly trees infested by scale insects. **Functional Ecology**, v. 18, n. 5, p. 664–669, 2004.

ROSSATO, J. A. DE S.; COSTA, G. H. G.; MADALENO, L. L.; MUTTON, M. J. R.; HIGLEY, L. G.; FERNANDES, O. A. Characterization and impact of the sugarcane borer on sugarcane yield and quality. **Agronomy Journal**, v. 105, n. 3, p. 643–648, 2013.

ROSSATO, J. A. S.; MADALENO, L. L.; MUTTON, M. J. R.; HIGLEY, L. G.; FERNANDES, O. A. Photosynthesis, yield and raw material quality of sugarcane injured by multiple pests. **PeerJ**, v. 2019, n. 1, p. e6166, 2019.

SANDHU, H. S.; CHERRY, R. H. Sugarcane borer, *Diatraea saccharalis* (F.) (Lepidoptera: Crambidae), injury and survival in energy cane versus sugarcane. **Sugar Tech**, v. 20, n. 5, p. 558–565, 2018.

SATHYABHAMA, M.; VISWANATHAN, R.; NANDAKUMAR, M.; MALATHI, P.; RAMESH SUNDAR, A. Understanding sugarcane defence responses during the initial phase of *Colletotrichum falcatum* pathogenesis by suppression subtractive hybridization (SSH). **Physiological and Molecular Plant Pathology**, v. 91, p. 131–140, 2015.

SAVI, T.; GARCÍA GONZÁLEZ, A.; HERRERA, J. C.; FORNECK, A. Gas exchange, biomass and non-structural carbohydrates dynamics in vines under combined drought and biotic stress. **BMC Plant Biology**, v. 19, n. 1, p. 1–11, 2019.

SAVITZKY, A.; GOLAY, M. J. Smoothing and differentiation of data by simplified least squares procedures. **Analytical chemistry**, v. 36, n. 8, p. 1627–1639, 1964.

SIDDIQUE, Z.; JAN, S.; IMADI, S. R.; GUL, A.; AHMAD, PARVAIZ. Drought stress and photosynthesis in plants. *Em*: AHMAD, P. (Ed.). . **Water Stress and Crop Plants: A Sustainable Approach**. West Sussex, UK: John Wiley & Sons, 2016. v. 1p. 1–11.

TAIZ, L.; ZEIGER, E.; MOLLER, I. M.; MURPHY A. **Plant physiology and development**. 6. ed. Sunderland, USA: Sinauer Asssociates, 2015.

TOMAZ, A. C.; COUTINHO, A. E.; SOARES, B. O.; PETERNELLI, L. A.; PEREIRA, E. J. G.; BARBOSA, M. H. P. Assessing resistance of sugarcane varieties to sugarcane borer *Diatraea saccharalis* Fab. (Lepidoptera: Crambidae). **Bulletin of Entomological Research**, v. 108, n. 4, p. 547–555, 2018.

VOHLAND, M.; BESOLD, J.; HILL, J.; FRÜND, H. C. Comparing different multivariate calibration methods for the determination of soil organic carbon pools with visible to near infrared spectroscopy. **Geoderma**, v. 166, n. 1, p. 198–205, 2011.

WAITE, T. A.; CAMPBELL, L. G. Controlling the false discovery rate and increasing statistical power in ecological studies. **Écoscience**, v. 13, n. 4, p. 439–442, 2006.

WELTER, S. C. Arthropod impact on plant gas exchange. *Em*: BERNAYS, E. A. (Ed.). **Insect-Plant Interactions**. 1. ed. Boca Raton, USA: CRC Press, 1989. p. 135–164.

YUAN, L.; BAO, Z.; ZHANG, H.; ZHANG, Y.; LIANG, X. Habitat monitoring to evaluate crop disease and pest distributions based on multi-source satellite remote sensing imagery. **Optik**, v. 145, p. 66–73, 1 set. 2017.

ZHANG, J.; HUANG, Y.; PU, R.; GONZALEZ-MORENO, P.; YUAN, L.; WU, K.; HUANG, W. Monitoring plant diseases and pests through remote sensing technology: a review. **Computers and Electronics in Agriculture**, v. 165, p. 104943, 2019.

ZHONG, J.; ZHANG, J.; ZHANG, Y.; GE, Y.; HE, W.; LIANG, C.; GAO, Y.; ZHU, Z.; MACHADO, R. A. R.; ZHOU, W. Heat stress reprograms herbivory-induced defense responses in potato plants. **BMC Plant Biology**, v. 24, n. 1, p. 1–18, 2024.

Supplementary Table 1. Mixed Linear Models (MLM) candidates tested by likelihood ratio test for gas exchange parameters. Each candidate model is compared with the simplest model (additive) and is selected only if $p < 0.05$

Parameter	Candidate model*	No. parameterers	AIC	BIC	$\chi 2$	df	P value
Ci	Ci= β0 + β1VARIETYijk * β2STRESSORSijk * β3DPIijk + ui + εijk	34	1943.8	054.6	24.19	15	0.06188
	Ci= β0 + β1VARIETYijk * β2STRESSORSijk + β3DPIijk + ui + εijk	13	1936.6	1978.9	4.49	3	0.21290
	Ci= β0 + β1VARIETYijk + β2STRESSORSijk * β3DPIijk + ui + εijk	19	1938.0	1999.9	10.53	6	0.10387
	Ci= β0 + β1VARIETYijk + β2STRESSORSijk + β3DPIijk + ui + εijk	10	1935.1	1967.7			
E	E= β0 + β1VARIETYijk * β2STRESSORSijk * β3DPIijk + ui + εijk	34	9.06	119.81	29.47	15	0.17138
	E= β0 + β1VARIETYijk * β2STRESSORSijk + β3DPIijk + ui + εijk	13	-3.66	38.68	6.50	3	0.15917
	E= β0 + β1VARIETYijk + β2STRESSORSijk * β3DPIijk + ui + εijk	19	-0.93	60.96	9.27	6	0.15917
	E= β0 + β1VARIETYijk + β2STRESSORSijk + β3DPIijk + ui + εijk	10	-3.17	29.41			
gs	gs= β0 + β1VARIETYijk * β2STRESSORSijk * β3DPIijk + ui + εijk	34	83.83	194.59	21.97	15	0.10856
	gs= β0 + β1VARIETYijk * β2STRESSORSijk + β3DPIijk + ui + εijk	13	74.62	116.96	9.16	3	0.06274
	gs= β0 + β1VARIETYijk + β2STRESSORSijk * β3DPIijk + ui + εijk	19	75.81	37.81	10.81	6	0.09443
	gs= β0 + β1VARIETYijk + β2STRESSORSijk + β3DPIijk + ui + εijk	10	77.78	110.35			

*$u_i \sim N(0, \sigma_u^2)$, $\varepsilon_{ijk} \sim N(0, \sigma^2)$

Supplementary Table 1 (continuation)

Parameter	Candidate model*	No. parameterers	AIC	BIC	$\chi 2$	df	P value
VPD	$VPD = \beta_0 + \beta_1 VARIETY_{ijk} * \beta_2 STRESSORS_{ijk} * \beta 3DPI_{ijk} + u_i + \varepsilon_{ijk}$	34	14.42	125.17	6.62	15	0.9674
	$VPD = \beta_0 + \beta_1 VARIETY_{ijk} * \beta_2 STRESSORS_{ijk} + \beta 3DPI_{ijk} + u_i + \varepsilon_{ijk}$	13	-10.42	31.92	1.65	3	0.6486
	$VPD = \beta_0 + \beta_1 VARIETY_{ijk} + \beta_2 STRESSORS_{ijk} * \beta 3DPI_{ijk} + u_i + \varepsilon_{ijk}$	19	-8.97	52.93	10.54	6	0.1036
	$VPD = \beta_0 + \beta_1 VARIETY_{ijk} + \beta_2 STRESSORS_{ijk} + \beta 3DPI_{ijk} + u_i + \varepsilon_{ijk}$	**10**	**-14.78**	**17.80**			
WUE	$WUE = \beta_0 + \beta_1 VARIETY_{ijk} * \beta_2 STRESSORS_{ijk} * \beta 3DPI_{ijk} + u_i + \varepsilon_{ijk}$	34	506.40	617.15	21.96	15	0.1088
	$WUE = \beta_0 + \beta_1 VARIETY_{ijk} * \beta_2 STRESSORS_{ijk} + \beta 3DPI_{ijk} + u_i + \varepsilon_{ijk}$	13	491.57	533.92	5.58	3	0.1339
	$WUE = \beta_0 + \beta_1 VARIETY_{ijk} + \beta_2 STRESSORS_{ijk} * \beta 3DPI_{ijk} + u_i + \varepsilon_{ijk}$	19	498.36	560.25	5.21	6	0.5169
	$WUE = \beta_0 + \beta_1 VARIETY_{ijk} + \beta_2 STRESSORS_{ijk} + \beta 3DPI_{ijk} + u_i + \varepsilon_{ijk}$	**10**	**491.15**	**523.73**			
A	$A = \beta_0 + \beta_1 VARIETY_{ijk} * \beta_2 STRESSORS_{ijk} * \beta 3DPI_{ijk} + u_i + \varepsilon_{ijk}$	34	1227.1	1337.8	10.89	15	0.76
	$A = \beta_0 + \beta_1 VARIETY_{ijk} * \beta_2 STRESSORS_{ijk} + \beta 3DPI_{ijk} + u_i + \varepsilon_{ijk}$	13	1199.3	1241.7	2.53	3	0.4692
	$A = \beta_0 + \beta_1 VARIETY_{ijk} + \beta_2 STRESSORS_{ijk} * \beta 3DPI_{ijk} + u_i + \varepsilon_{ijk}$	19	1208.0	1269.9	3.37	6	0.7610
	$A = \beta_0 + \beta_1 VARIETY_{ijk} + \beta_2 STRESSORS_{ijk} + \beta 3DPI_{ijk} + u_i + \varepsilon_{ijk}$	**10**	**1195.9**	**1228.5**			

*$u_i \sim N(0, \sigma_u^2)$, $\varepsilon_{ijk} \sim N(0, \sigma^2)$

Supplementary Table 2. Estimate of gas exchange parameters for the selected mixed linear model

Parameter	Term	Estimate	SD	df	t value	P value
Ci	**Intercept**	**181.30**	**7.63**	**86.068**	**23.76**	**$2.00\ 10^{-16}$**
	Variety (CTC 4)	**29.63**	**6.24**	**43**	**4.75**	**$2.29\ 10^{-5}$**
	NSDS	-4.68	8.93	43	-0.52	0.6029
	WSC	**-19.75**	**8.25**	**43**	**-2.39**	**0.0211**
	WSDS	-8.88	8.66	43	-1.03	0.3108
	8 DPI	5.97	6.99	141	0.85	0.3947
	13 DPI	-13.63	6.99	141	-195	0.0533
	18 DPI	-6.09	6.99	141	-0.87	0.3855
E	**Intercept**	**1.95**	**0.05**	**80.85**	**38.59**	**$2.00\ 10^{-16}$**
	Variety (CTC 4)	**0.25**	**0.042**	**43**	**6.05**	**$2.00\ 10^{-16}$**
	NSDS	**-0.14**	**0.060**	**43**	**-2.26**	**0.0289**
	WSC	**-0.20**	**0.056**	**43**	**-3.67**	**0.00067**
	WSDS	**-0.17**	**0.058**	**43**	**-2.84**	**0.0069**
	8 DPI	**-0.27**	**0.044**	**141**	**-6.16**	**$7.32\ 10^{-9}$**
	13 DPI	**-0.32**	**0.044**	**141**	**-7.18**	**$3.66\ 10^{-11}$**
	18 DPI	**-0.27**	**0.044**	**141**	**-6.18**	**$6.36\ 10^{-9}$**
gs	**Intercept**	**5.69**	**0.061**	**84.59**	**93.24**	**$2.00\ 10^{-16}$**
	Variety (CTC 4)	**0.38**	**0.050**	**43**	**7.61**	**$1.68\ 10^{-9}$**
	NSDS	**-0.18**	**0.071**	**43**	**-2.50**	**0.0161**
	WSC	**-0.25**	**0.066**	**43**	**-3.83**	**0.00041**
	WSDS	**-0.21**	**0.070**	**43**	**-3.07**	**0.0036**
	8 DPI	**-0.13**	**0.055**	**141**	**-2.32**	**0.021**
	13 DPI	**-0.28**	**0.055**	**141**	**-5.02**	**$1.51\ 10^{-6}$**
	18 DPI	**-0.24**	**0.055**	**141**	**-4.36**	**$2.46\ 10^{-5}$**

Supplementary Table 2 (continuation)

Parameter	Term	Estimate	SD	df	t value	P value
VPD	**Intercept**	**2.39**	**0.059**	**60.80**	**40.26**	**$2.00\ 10^{-16}$**
	Variety (CTC 4)	**-0.19**	**0.053**	**43**	**-3.64**	**0.00073**
	NSDS	0.079	0.077	43	1.03	0.3104
	WSC	0.095	0.071	43	1.35	0.1857
	WSDS	0.080	0.074	43	1.075	0.2885
	8 DPI	**-0.30**	**0.039**	**141**	**-7.66**	**$2.73\ 10^{-12}$**
	13 DPI	**-0.13**	**0.039**	**141**	**-3.37**	**0.000965**
	18 DPI	**-0.11**	**0.039**	**141**	**-3.00**	**0.003227**
WUE	**Intercept**	**4.43**	**0.17**	**96.41**	**26.05**	**$2.00\ 10^{-16}$**
	Variety (CTC 4)	**-0.42**	**0.13**	**43**	**-3.17**	**0.002818**
	NSDS	0.01	0.19	43	0.076	0.939394
	WSC	0.33	0.18	43	1.87	0.06786
	WSDS	0.13	0.19	43	0.71	0.4833
	8 DPI	**0.60**	**0.17**	**141**	**3.64**	**0.000384**
	13 DPI	**0.77**	**0.17**	**141**	**4.63**	**$8.36\ 10^{-6}$**
	18 DPI	**0.51**	**0.17**	**141**	**3.05**	**0.002706**
A	**Intercept**	**30.64**	**1.11**	**86.67**	**27.60**	**$2.00\ 10^{-16}$**
	Variety (CTC 4)	**4.27**	**0.90**	**43**	**4.72**	**$2.54\ 10^{-5}$**
	NSDS	**-3.60**	**1.30**	**43**	**-2.78**	**0.008099**
	WSC	**-3.55**	**1.20**	**43**	**-2.96**	**0.004934**
	WSDS	**-3.58**	**1.26**	**43**	**-2.85**	**0.006729**
	8 DPI	**-2.92**	**1.02**	**141**	**-2.86**	**0.004939**
	13 DPI	**-3.81**	**1.02**	**141**	**-3.73**	**0.000276**
	18 DPI	**-4.27**	**1.02**	**141**	**-4.18**	**$5.07\ 10^{-5}$**

Supplementary Table 3. ANOVA table from Mixed Linear Models (MLM) considering the effects of sugarcane varieties, biotic and abiotic stressors and time after sugarcane borer infestation (DPI) on gas exchange parameters

Response*	Source of variation	Sum of squares	Mean square	df	F	P value	η_p^2**
	Variety	**26487.0**	**26487.0**	**1**	**22.5623**	**$2.29\ 10^{-5}$**	**0.34**
Ci	Treatment	7177.5	2392.5	3	2.038	0.12	0.12
	DPI	**10137.4**	**3379.1**	**3**	**2.8784**	**0.04**	**0.06**
	Variety	**1.72**	**1.72**	**1**	**36.62**	**$3.04\ 10^{-7}$**	**0.46**
E	**Treatment**	**0.72**	**0.24**	**3**	**5.08**	**$4.2\ 10^{-3}$**	**0.26**
	DPI	**3.05**	**1.02**	**3**	**21.62**	**$1.4\ 10^{-11}$**	**0.32**
	Variety	**4.25**	**4.25**	**1**	**57.97**	**$1.68\ 10^{-9}$**	**0.57**
gs	**Treatment**	**1.25**	**0.42**	**3**	**5.70**	**0.0022**	**0.28**
	DPI	**2.25**	**0.75**	**3**	**10.26**	**$3.75\ 10^{-6}$**	**0.18**
	Variety	**0.49**	**0.49**	**1**	**13.24**	**$7.2\ 10^{-4}$**	**0.24**
VPD	Treatment	0.081	0.027	3	0.73	0.54	0.05
	DPI	**2.20**	**0.73**	**3**	**19.88**	**$8.39\ 10^{-11}$**	**0.30**
	Variety	**6.74**	**6.74**	**1**	**10.04**	**$2.82\ 10^{-3}$**	**0.19**
WUE	Treatment	2.85	0.95	3	1.41	0.25	0.09
	DPI	**16.03**	**5.34**	**3**	**7.96**	**$6.12\ 10^{-5}$**	**0.14**
	Variety	**492.83**	**492.83**	**1**	**17.85**	**$1.21\ 10^{-4}$**	**0.29**
A	**Treatment**	**258.12**	**86.04**	**3**	**3.12**	**0.036**	**0.18**
	DPI	**426.18**	**142.06**	**3**	**5.15**	**$2.01\ 10^{-3}$**	**0.10**

*Ci - CO_2 Intercellular concentration; E - Transpiration; gs - stomach conductivity; VPD - vapor pressure deficit from the leaf to air; WUE - Water use efficiency in photosynthesis; A - assimilation/respiration.**η_p^2: Partial variance explained

CHAPTER 3 – Comparison of multispectral remote sensing platforms for sugarcane billbug attack (Coleoptera: Curculionidae) detection: a proposal for sampling optimization

Resumo

Métodos manuais de monitoramento contínuo de pragas são difíceis de serem implementados na cultura da cana-de-açúcar devido ao esforço empregado por monitores. Como consequência, a frequência de amostragem adotada por produtores é insuficiente para permitir medidas oportunas de controle das pragas, especialmente para o bicudo-da-cana, *Sphenophorus levis* Vaurie, 1978. O uso de tecnologias, como sensoriamento remoto, permite obter respostas sobre o estado sanitário da cultura sem estar em contato físico, agilizando a tomada de decisão. Neste trabalho, modelos de *machine learning* foram ajustados para compreender o efeito do ataque do bicudo-da-cana através de características espectrais extraídas de sensores multiespectrais embarcados em VANT's (veículos aéreos não tripulados) e satélites. Amostragens tradicionais do bicudo-da-cana foram realizadas mensalmente durante cinco meses em três canaviais comerciais, avaliando-se três pontos aleatórios por parcela para contagem de colmos injuriados, o número total de colmos, e a quantidade de larvas, pupas e adultos dentro dos colmos de cana. Imagens provenientes de sensores multiespectrais foram obtidas em intervalos próximos à amostragem. Após o devido processamento, informações derivadas das bandas puras como índices de vegetação, componentes principais, e atributos da matriz de co-ocorrência de nível de cinza dos dois sistemas foram calculados. Os dados gerados de cada parcela foram extraídos e mesclados aos dados de campo para modelagem via Modelos Lineares Generalizados Mistos (GLMM's) e algoritmos de *machine learning*. Os GLMM's demonstram diferenças significativas entre níveis de infestação, embora tais diferenças dependam da variedade, banda e sensor (plataforma) considerado. As árvores de decisão representados pelo *Random forest* e *Extreme Gradient Boosting Trees*, se destacaram entre os algoritmos com maior poder preditivo para os dados provenientes do VANT e satélite respectivamente. Em ambas as plataformas, algoritmos ajustados aos dados referentes aos primeiro e segundo meses de avaliação, em que as plantas possuíam menor índice de área foliar (IAF), tiveram melhores resultados. As duas plataformas tiveram métricas satisfatórias de predição, embora os dados de origem orbital foram mais eficazes na predição (VANT: RMSE = 2.05 e R^2 = 0.69; satélite: RMSE = 1.68 e R^2 = 0.80). A iniciativa pioneira utilizando sensoriamento remoto aéreo e orbital para detectar infestações do bicudo-da-cana demonstra alguns desafios a serem superados. Ainda assim, os resultados encontrados representam um primeiro passo para o aprimoramento do monitoramento em grande escala do bicudo-da-cana, potencializando a tomada de decisão de controle desta praga-chave da cana-de-açúcar.

Palavras-chave: agricultura digital, aprendizado de máquina, manejo integrado de pragas de precisão, tomada de decisão.

Abstract

In sugarcane crops, manual sampling methods for continuous pest monitoring are difficult to implement due to the effort employed by scouters. Consequently, the sampling frequency adopted by growers is insufficient to allow timely pest control measures, especially for the sugarcane billbug, *Sphenophorus levis* Vaurie, 1978. The use of technologies such as remote sensing allow to obtain answers about crop health status without being in physical contact, speeding up decision-making. As part of this study, we adjusted machine learning models to understand the effect of the sugarcane billbug attack using spectral characteristics extracted from multispectral sensors embedded in UAVs and satellites. Traditional billbug samplings were carried out monthly in three commercial sugarcane fields for five months, evaluating three random points per plot to count injured stalks, the total number of stalks, and the quantity of larvae, pupae, and adults inside sugarcane stumps. Images from multispectral sensors were taken close to sampling intervals. After due processing, information derived from the bands, such as vegetation indices, principal components, and gray level co-occurrence matrix attributes of the two platform systems, was calculated. The data generated from each plot was extracted and merged with field data for modeling through Generalized Linear Mixed Models (GLMMs) and machine learning algorithms. The GLMMs revealed significant differences between infestation levels, although such differences depend on the sugarcane variety, band, and sensor (platform) system. Decision trees, represented by Random Forest and Extreme Gradient Boosting Trees, stood out among the algorithms with the greatest predictive power for data from UAVs and satellites, respectively. On both platforms, algorithms fitted to data referring to the first and second sampling months, where the plants had a lower leaf area index (LAI), had better results. Both platforms had satisfactory prediction metrics, although orbital data were more effective in prediction (UAV: RMSE = 2.05 and R^2 = 0.69; satellite: RMSE = 1.68 and R^2 = 0.80). The pioneering initiative using aerial and orbital remote sensing to detect sugarcane billbug infestations exhibits some challenges to be overcome. Even so, the results represent a first step towards improving large-scale monitoring of the sugarcane billbug, enhancing decision-making to control this key sugarcane pest.

Keywords: decision making, digital agriculture, machine learning, precision pest management.

Introduction

Pest sampling is a crucial step in the Integrated Pest Management (IPM) programs. Surveys about the pest infestation level provide growers with information for more rational decision-making, saving time and resources (Dara, 2019). Traditional monitoring methods in IPM to collect data are manually based on regular field scouting (Higley e Pedigo, 1996). Although effective, these surveys are time-consuming, laborious, limited to smaller areas, and may be prone to errors if the scouter is not well trained (Preti, Verheggen and Angeli, 2021). Moreover, most surveys still ignore the inclusion of georeferenced observation data, which allows a better understanding of the ecological processes involved in pest population dynamics and even localized control strategies (Karimzadeh and Sciarretta, 2022; Silva *et al.*, 2023; Rosa, Soares and Fernandes, 2024; Zhou *et al.*, 2024). Therefore, accurate and up-to-date space-time information on the presence and dynamics of pest infestations is essential for efficient and effective decision-making (Peterson, Higley and Pedigo, 2018; Dara, 2019; Zhou *et al.*, 2024).

The sugarcane crop (*Saccharum* spp.) is a challenging environment for continuous pest monitoring. Consequently, the sampling frequency adopted by growers is insufficient to implement timely pest control measures (Reagan e Mulcahy, 2019). A relevant example is the sugarcane billbug, *Sphenophorus levis* Vaurie, 1978 (Coleoptera: Curculionidae), a rhizome and culm borer insect. Sugarcane billbug larvae cause progressive yellowing and eventually the death of sugarcane tillers by consuming the tissue of young plants (Dinardo-Miranda, 2005).

The sampling scheme for the sugarcane billbug population is laborious, making it difficult to scout it on a large scale (Pavlu *et al.*, 2016; Xavier *et al.*, 2024). The sampling process entails removing rhizomes through trenches and opening the remains of culms with machetes for visual inspection, accounting for the presence of biological forms (larvae, pupae, and adults) and injuries (Dinardo-Miranda, 2005). A skillful scouter can evaluate, on average, one clump every six minutes, excluding the time for walking between sample points. In addition, most growers and plants adopt a sample density of two points per hectare, which may be insufficient to detect initial infestations (Alencar, 2016; Xavier *et al.*, 2024). In view of the effort required and the difficulty in allocating human resources, many growers limit the sampling frequency to once a year, immediately after harvesting. Meanwhile, field observations of the

sugarcane billbug's spacetime dynamics reveal overlapping generations, reinforcing the need to intensify sampling.

In the Digital Agriculture era, technology adoption allows for faster decision-making. Sensor-derived data, whether coupled to Internet of Things (IoT) platforms and devices, can assist growers and technicians in identifying, monitoring, and even choosing control tactics through artificial intelligence (Barbedo, 2019). Remote sensing is one of the new proposals for monitoring pest attacks (Nansen, 2016; Nansen and Elliott, 2016; Zhang *et al.*, 2019; Rhodes *et al.*, 2022). Images obtained by sensors embedded in unmanned aerial vehicles (UAVs) and multispectral satellites can provide answers about the sanitary state of the crop without being in physical contact with plants (Nansen and Elliott, 2016; Zhang *et al.*, 2019). In this way, it is possible to successfully map areas attacked by insects promptly and non-invasively (Vanegas *et al.*, 2018; Barbedo, 2019; Rhodes *et al.*, 2022; Mahanta *et al.*, 2024).

In this work, we applied machine learning models to predict the attack of the sugarcane billbug using spectral characteristics extracted from images of multispectral sensors embedded in UAVs and satellites. Our objective was to investigate the suitability of the two platforms for the monitoring of sugarcane billbug, uncovering what information is relevant for their identification and potentially applicable for large-scale detection.

Materials and Methods

The research was carried out on three commercial sugarcane fields located in the municipalities of Barrinha and Itirapina, São Paulo state, Brazil (**Figure 4**), comprising the growing seasons of 2022/2023 and 2023/2024.

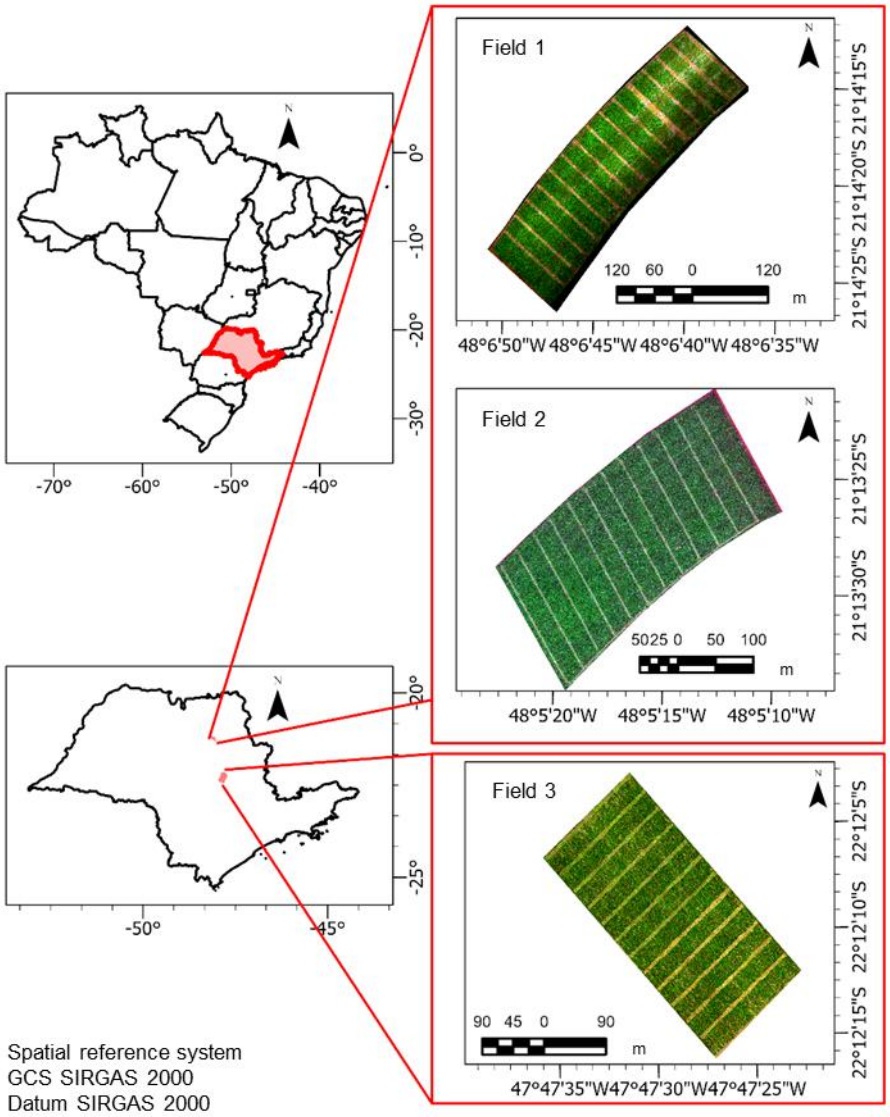


Figure 4 – Location of the experimental fields in the municipalities of Barrinha (Fields 1 and 2) and Itirapina (Field 3), São Paulo, Brazil.

In the experimental areas, different management strategies were evaluated for controlling sugarcane billbug. Two insecticide application modes, known as tiller cutter and localized vinasse, and seven different insecticides were tested on an area of approximately 6 ha. Consequently, the spectral response of plants could potentially visualize a heterogeneous infestation gradient.

All agronomic management practices were carried out according to technical recommendations, except for the control of sugarcane billbug. The implementation of the experiment was carried out at the beginning of the rainy season in November 2022 for the 2022/2023 growing season (field 1) grown with the variety CTC 2994 and in October and November 2023 for the growing season 2023/2024 (fields 2 and 3) grown

with varieties RB 005014 and CTC 1007, respectively (**Table 4**). In the 2022/2023 growing season, the experiment consisted of 64 plots 25 m long and 18 m wide. Twelve sugarcane lines, spaced 1.5 m apart, comprised each plot, resulting in a total area of 450 m^2. The growing season of 2023/2024 retained the 64 plots, but with an increase of 4 cane lines per plot, totaling an area of 600 m^2.

The application of the sugarcane billbug control treatments was carried out at the beginning of the rainy season in November 2022 for the 2022/2023 crop season (field 1), and in October and November 2023 for fields 2 and 3, respectively, for the 2023/2024 crop season. We carried out monthly sampling, evaluating three random points per plot (**Table 4**). The sampling consists of the removal of the clumps randomly selected between rows 3 and 4 and 9 and 10 (2022/2023 growing season) or 13 and 14 (2023/2024 growing season). After removing the rhizome from the trenches with a mattock, the reminiscent culms (hereafter stumps) were cut longitudinally with a machete (Xavier *et al.*, 2024). A careful inspection quantified the number of injured stumps, the total number of stumps, and the number of biological forms (larvae, pupae, and adults inside the stumps). During the information recording process, other soil pests such as the sugarcane hairy borer *Hyponeuma taltula* (Schaus, 1904) (Lepidoptera: Erebidae), another sugarcane rhizome pest, were identified as the cause of the injury. Sugarcane billbug injury is characterized by the presence of clear-colored feces containing fine fibers inside the tunnels, while the sugarcane hairy borer leaves no apparent debris in the tunnels. We calculated the proportion of attacked stumps (AS) from these values by dividing the number of attacked stumps by the total number of evaluated stumps.

Table 4. Dates of sugarcane billbug sampling conducted in the experimental areas

Growing season	Field	Variety	Sampling	Sampling dates
2022/2023	1	CTC 2994	1	14/12/2022
			2	12/01/2023
			3	16/02/2023
			4	16/03/2023
			5	20/04/2023
2023/2024	2	RB 005014	1	28/09/2023
			2	10/11/2023
			3	11/12/2023
			4	11/01/2024
			5	16/02/2024
	3	CTC 1007	1	16/10/2024
			2	05/12/2024
			3	18/01/2024
			4	22/02/2024
			5	26/03/2024

Multispectral UAV image acquisition

We installed control and check points before the first flight in each experimental area, then used a geodesic survey to obtain their coordinates using dual-frequency GNSS receivers (L1/L2). The control points consisted of white-colored targets that were positioned at ground level and distributed throughout the experimental area. During image processing, we used these points' known coordinates as a reference to correct potential distortions and inaccuracies, thereby ensuring the image's positional accuracy.

We positioned a dual-frequency GNSS (L1/L2) as a base for post-processing and georeferencing images during the flight, in addition to the control points. The flights were carried out on the day the samples were taken, or within a margin of ± 5 days if weather conditions did not allow them. The Agrowing® multispectral A7Rv sensor was used. This sensor captures 14 bands between the visible and near-infrared spectrums (**Table 5**). We coupled the sensor to the DJI Matrice 300 RTK UAV, adapting it with a dual-frequency antenna for positioning correction via Post-Processed Kinematics (PPK). Flights were conducted between 10:00 a.m. and 3:00 p.m. on all assessment dates (Khaliq *et al.*, 2019). The "DJI pilot2" app was used to define the flight plans, which included a 70% lateral and 60% frontal overlap rate, a flight altitude of 150 m, and an approximate ground sampling distance (GSD) of 2.6 cm pixel^{-1}. In the road, next to the plots, two Ethylene Vinyl Acetate (EVA) targets in white, black, light gray,

and dark gray colors were placed at the beginning and end of the UAV flight trajectory for subsequent radiometric calibration.

Before data extraction, a careful inspection was carried out on the orthomosaics to detect possible cloud-covered plots, and if this occurrence had been detected, their information was disregarded in successive stages. Due to the application of limestone that affected plant leaves and sensor settings, the first flight of Field 1 (December 2022) was disregarded from processing.

Table 5. Features of the bands of the Agrowing® multispectral sensor

Band (nm)	FWHM*
405	15,80
430	17,56
450	16,81
490	16,19
525	17,43
550	15,86
560	16,61
630	14,83
570	16,26
630	18,95
686	16,28
710	18,10
735	19,87
850	20,29
ISO	100
Shutter speed	1:640
Radiometric resolution	8 bits

*FWHM: Full width at half height

Multispectral satellite image acquisition

PlanetScope® orbital images were used following the same period when field data was collected for each assessment date and experimental fields (3 fields, 5 months [images] each, totaling 15 images). The nanosatellite constellation uses a multispectral instrument (eight spectral channels) with a range width of 25 km and high radiometric and spatial resolution, storing information in 16 bits with GSD of approximately 3.5 m pixel^{-1}. In this study, the eight available bands were considered (**Table 6**). All images were researched and acquired by the “Planet Imagery” plugin via the ArcGIS Pro® software (access via the institutional account – jrs.soares@unesp.br_unesp_edu) through the Planet Labs Education and Research

Program. The sensor on board internally orthorectifies and scales the original images to the top of the atmospheric radiance. The screening of the images followed the criteria of cloud coverage level (< 1%) and the availability of the image on the sampling date. If this condition was not met, the image immediately closest to sampling was selected at an interval of ± 5 days. The selected images were then cut according to the boundaries of the experimental field and radiometrically harmonized if the scene was captured by more than one satellite.

Table 6. Features of the bands provided by the PlanetScope® instruments

Band	Wavelenght (nm)	FWHM*
Coastal blue	443	20
Blue	490	50
Green I	531	36
Green	565	36
Yellow	610	20
Red	665	31
Red Edge	705	15
Near-infrared	865	40

*FWHM: Full width at half height

Image and vector files processing

The images and vector layers were projected in the WGS/UTM zones 22S (fields 1 and 2) and 23S (field 3) using a GIS software. The vector layers of the plots were created in ArcGIS Pro® from the Agrowing® georeferenced high-resolution RGB image composition. An internal buffer of 3 m was applied to the boundaries of each plot to exclude possible border effects and ensure that the spectral data corresponded to the corresponding plot.

After each flight, the Agrowing® images and GNSS files from the base and the UAV were transferred to the computer for processing. The initial processing involved the individual georeferencing of images ("geotagging") via PPK processing. Preliminarily, the position of the field base was corrected using the base of the Brazilian Continuous Monitoring Network (RBMC) of the Brazilian Institute of Geography and Statistics (IBGE) closest to the overflight area as a reference (Jaboticabal, code: SPJA; São Carlos, Code: EESC). Subsequently, the UAV trajectory correction was implemented using the newly corrected field base position. The coordinates of the images were defined using the T2R Geotagger software (T2R Soluções Tecnológicas,

2024). In the software were imported the images in RAW format and native files (ubx extension) and the post-processed trajectory of the UAV flight. As processing output, a list of the coordinates of each flight image was generated.

The RAW images were subsequently imported into the Agrowing Basics® software provided by the sensor manufacturer. In this step, the images were conferred on the alignment of pixels between the bands, ensuring that there was the correct overlap between them. The images imported into the software had an automatic pre-alignment of the bands, but on all flights, the quality of this alignment was checked, and manual corrections were performed when necessary. Then the 14 bands of the RAW images were extracted, saving them in “tiff” format with 8-bit resolution and the “Auto Gamma” correction option disabled.

The aligned and extracted images of each band were phototriangulated in the Agisoft Metashape® software using the corrected coordinate list and the control points collected during the geodesic survey. The result was an orthomosaic containing all 14 bands for each sampling date.

The radiometric calibration of the orthomosaics was carried out by the empirical line method (Smith and Milton, 1999). At this stage, we generated regions of interest (ROIs) on the EVA plates for the extraction of the digital number (DN) values in the ArcGIS Pro® software. The ASD FieldSpec® HandHeld UV/NIR model spectroradiometer (ASD, 2002), which collects spectral data in the range of 325 nm to 1075 nm with a sample range of 1.6 nm, was used to pre-define target reflectance. The measurements of the EVA targets were taken in a dark room with the help of halogen lamps to ensure constant illumination. A lens with a field of view (FOV) of 1° was attached to the equipment. Each target's reflection has been band-simulated to match the central and FMWH bands of the Agrowing® sensor. Then, the DN of the ROIs of each target and band were paired with the respective values obtained in the band simulation for obtaining the calibration coefficients (i.e., angular and constant) in

Excel (**Figure 5**). The regression coefficient values obtained were entered in the ArcGIS Pro® raster calculator for conversion for each band's reflection factor.

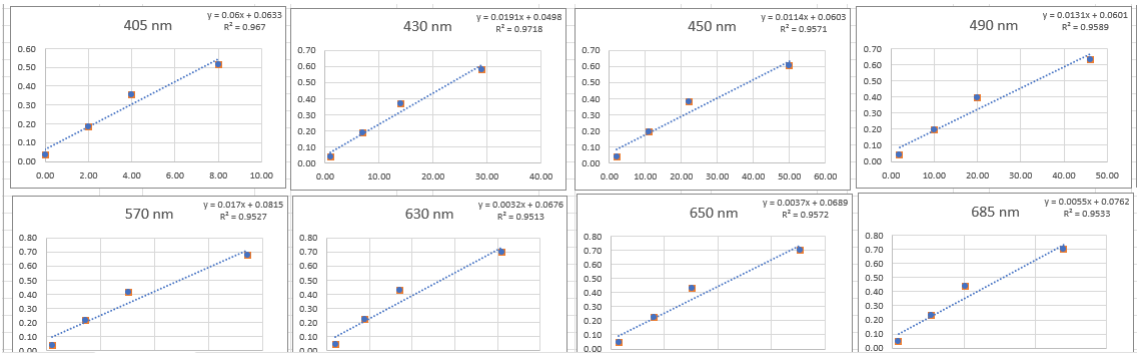


Figure 5 – Example of radiometric calibration adjustment by empirical line method.

Then the corrected images from Agrowing® and Planet® were imported into R software version 4.2.1 (R Core Team, 2022). To speed up the processing of Agrowing® images, a resampling of pixels with a four-fold aggregation factor was performed, which resulted in approximately 10.4 cm pixel^{-1} final GSD in the images. Among the further processing carried out were the calculation of vegetation indices (**Table 7**) and the extraction of the first three main components (PCs). The vegetation indices and PCs were calculated using the "RSToolbox" package version 0.4.0 (Leutner *et al.*, 2024) and "Pliman" version 2.1.0.9 (Olivoto, 2022).

Table 7. Formulae for calculation of the vegetation indices

Indices*	Formula
CTVI	$\frac{\mathrm{NDVI}+0{,}5}{\lvert \mathrm{NDVI}+0{,}5\rvert}\cdot\sqrt{\lvert(\mathrm{NDVI})+0{,}5}$
DVI**	$s*NIR-RED$
EVI**	$G*-\frac{NIR-RED}{NIR+C1*RED-C2*BLUE+Levi)}$
GEMI	$\frac{(NIR^2+RED^2)*2+(NIR*1{,}5)+(RED*0{,}5)}{(NIR+RED+0{,}5)*\left(1-(NIR^2+RED^2)*2+(NIR*1{,}5)+(RED*0{,}5)\right.}$
GNDVI	$\frac{\mathrm{NIR}-\mathrm{GREEN}}{\mathrm{NIR}+\mathrm{GREEN}}$
KNDVI	$\tan\left(\frac{NIR-RED}{NIR+RED}\right)^2$
MCARI	$(RED\ EDGE-RED)-0.2\,(RED\ EDGE-GREEN))\left(\frac{RED\ EDGE}{RED}\right)$
MSAVI	$(\mathrm{NIR}+0{,}5)-0{,}5*\sqrt{(2*\mathrm{NIR}+1)^2-8*(\mathrm{NIR}-2*\mathrm{RED})}$
MSAVI 2	$2*(\mathrm{NIR}+1)-\sqrt{\frac{(2*\mathrm{NIR}+1)^2-8*(\mathrm{NIR}-\mathrm{RED})}{2}}$
NDVI	$\frac{NIR-RED}{NIR+RED}$
NDWI	$\frac{GREEN-NIR}{GREEN+\ NIR}$
NRVI	$\frac{\frac{RED}{NIR}-1}{\frac{RED}{NIR}+1}$
RVI	$\frac{RED}{NIR}$
SAVI**	$\frac{(NIR-RED)*(1+L)}{(NIR+RED+L)}$
SR	$\frac{NIR}{RED}$
TTVI	$\sqrt{\frac{\lvert NIR-RED\rvert}{\lvert NIR+RED\rvert}+0{,}5}$
TVI	$\sqrt{\frac{NIR-RED}{NIR+RED}+0{,}5}$
WDVI**	$NIR-s*RED$

* CTVI: Corrected Transformed Vegetation Index; DVI: Difference Vegetation Index; EVI: Enhanced Vegetation Index: GEMI: Global Environmental Monitoring Index: GNDVI: Green Normalised Difference Vegetation Index; KNDVI: Kernel Normalised Difference Vegetation Index; MCARI: Modified Chlorophyll Absorption Ratio Index; MSAVI: Modified Soil Adjusted Vegetation Index; MSAVI2: Modified Soil Adjusted Vegetation Index 2; NDVI: Normalized difference vegetation index; NDWI: Normalised Difference Water Index; NRVI: Normalised Ratio Vegetation Index; RVI: Ratio Vegetation Index; SAVI: Soil Adjusted Vegetation Index; SR: Simple Ratio Vegetation Index; TTVI: Thiam's Transformed Vegetation Index; TVI: Transformed Vegetation Index; WDVI: Weighted Difference Vegetation Index.

** L = 0.5, G = 2.5, Levi = 1, C1 = 6, C2 = 7.5, s = 1

Additionally, image texture attributes were calculated using the Grayscale Co-occurrence Matrix (GLCM) (**Table 8**). The GLCM texture metrics consider the spatial relationship of neighboring pixel values, in which the value of a given pixel is based on a focal pixel and neighboring(s) (Haralick, Shanmugam and Dinstein, 1973). The GLCM analysis can display cluster behaviors between pixels, which justifies its use in this study since the sugarcane billbug has gregarian behavior and usually results in rebound-type failures in sugarcane fields (Pavlu and Molin, 2016; Rosa, Soares and Fernandes, 2024). For this analysis, eight metrics were calculated for each band and indices at each evaluation date (**Table 8**) for data generated by UAVs and satellites. For GLCM calculations, a window of 11x11 and 3x3 neighboring pixels, 16 and 32 gray levels scale, was considered for frequency quantification for Agrowing® and Planet® images, respectively. It was considered the "equal prob" quantization method to create quartiles and the calculation of the metric of interest considering an average of all directions (i.e., 0°, 45°, 90°, and 135°). GLCM attributes were calculated using the “GLCMTextures” package version 0.4.1 (Ilich, 2020).

Table 8. Grayscale Co-occurrence Matrix (GLCM) texture metrics calculated

Group	Metrics	Formula
Contrast	Contrast	$\sum_{i,j=0}^{N-1} P_{i,j}\,(i-j)^2$
	Dissimilarity	$\sum_{i,j=0}^{N-1} P_{i,j}\,\lvert i-j\rvert$
	Homogeneity	$\sum_{i,j=0}^{N-1} \frac{P_{i,j}}{1+(i-j)^2}$
Order	Angular second moment	$\sum_{i,j=0}^{N-1} P_{i,j}^2$
	Entropy**	$\sum_{i,j=0}^{N-1} P_{i,j} - \left[-\ln P_{i,j}\right]$
Descriptive	Mean	$\sum_{i,j=0}^{N-1} i\,P_{i,j}$
	Variance	$\sum_{i,j=0}^{N-1} P_{i,j}\,(i-\mu)^2$
	Correlation	$\sum_{i,j=0}^{N-1} P_{i,j}\,\frac{(i-\mu)*(j-\mu)}{\sigma^2}$
Other	Mean sum***	$\sum_{k=0}^{2N-1} k * k_{prob}$

* N = Number of lines or columns in the GLCM (equal to the number of gray levels)
i = line indices of the GLCM matrix (equal to the gray level of the reference cell)
j = GLCM matrix column indices (equal to neighbouring cell gray level)
$P_{i,j}$ = Probability (relative frequency) of adjacent cells with gray levels i and j
** 0 * ln(0) = 0
*** k=i+j, and k_{prob} are grey-level sum vectors. The grey level sum vector is a vector that represents the probability distribution of the sum of two grey levels (i+j) based on the calculated GLCM are grey-level sum vectors.

We filtered the soil-containing pixels from the Agrowing® sensor by creating a binary mask using the "Otsu" algorithm on the NDVI index. Masks were created for each flight, that is, for each experimental area and sampling month, and applied to all layers (bands, vegetation indices, PCs, and textural attributes).

The information generated by each sensor was stacked separately for the composition of a hypercube. Based on the information stacked, the average of the values of pixels in each layer of information (i.e., bands, vegetation indices, texture attributes, and PCs) was calculated considering the vector layers of the plots. The information extracted was combined with the data observed in the field for modeling in machine learning algorithms.

Data processing, analysis and implementation of machine learning models

For the purposes of visualization of spectral curves according to infestation and sampling date, data on the proportion of attacked stumps were classified according to

their infestation degree. The proportion of attacked stumps was separated into quartiles considering the data from the five surveys, and then four classes were created (% AS) (Low: 0.0–5.6% AS; Mean: 5.7–11% AS; High: 11.1–18.0% AS; Very high: 18.1–75.0% AS). Spectral profile graphs were created, which represent the average reflectance of the three areas (varieties) for each band, sampling month, and sensors studied.

Based on the information generated by UAVs and satellites, Generalized Linear Mixed Models (GLMM's) (Brooks *et al.*, 2017) were fitted to investigate possible differences in band reflectance between the different infestation levels, varieties, sampling month, and interactions between infesting classes and varieties. These models were adjusted using the Student t distribution family for the datasets generated by the UAV and satellite. Since these were repeated measurements from the same plots over sampling months, the influence of the plots nested in each area was considered a random effect. The normality and homogeneity of residuals was checked through the "DHARMA" package (Hartig, 2022). The effect of the factors was observed through the Wald type "III" test at 5% significance. Models that showed significant interaction between levels of infestation and variety were compared by fixing the sampling month, and the interaction was unfolded by the difference infestation classes in each variety by the Tukey test at 5% significance.

Prior to machine learning model adjustment, an exploratory analysis revealed that the infestation level observed in each sampling month had a greater correlation with the variables of the following month. Due to this observation and the population dynamics of the pest, in addition to the sugarcane phenology, the proportion of attacked stumps was converted to the area under the attack progress curve (AUC) before modeling (Alves *et al.*, 2017; Ruppel, 1984). The method for calculating the AUC considers the trapezoidal area that separates the proportion of attacked stumps between the sampling in month j and the subsequent sampling, as well as the difference in days between the samples for each plot i (Ruppel, 1984):

$$AUC_{i,j+1} = \left[\frac{(r_{i,j} + r_{i,j+1})}{2}\right] * \left(T_{i,j+1} - T_{i,j}\right),$$

where $r_{i,j}$ is the proportion of attacked stumps observed in plot i in sampling month j, $r_{i,j+1}$ is the proportion of attacked stumps observed in plot i, of the subsequent sampling, and $T_{i,j+1} – T_{i,j}$ is the difference in days between the two sequential samples for plot i.

After calculating the area for each month, the areas are then summed to generate the pest attack progress curves (Ruppel, 1984):

$$AUC_{cumulative} = \sum_{i,j+1} AUC_{i,j} + AUC_{i,j+1}$$

The total dataset consisted of sampling months, varieties of sugarcane grown in each field, reflectance values of the spectral bands, PCs, vegetation indices, and textural attributes of the bands and vegetation indices. To determine which time in sugarcane phenology returns the best results, the dataset was divided by considering the cumulative data in sequence, i.e., the AUC between the first sampling month and the second month, the first month and the third month, until the observations of all dates are incorporated (**Table 10** and **Table 13**). We decided to test such periods because, normally, from a certain point of development, sugarcane shows a behavior of saturation or stability in its spectral profile and the seasonality of the pest population (**Figure 6** and **Supplementary Figure 1**). These phenomena can negatively influence the predictive power of models.

The adjustment of predictive models was implemented using the “Tidymodels” package version 1.1.1 (Kuhn and Wickham, 2020). In each subset, the data were randomly divided for training and testing of the models, considering an 80:20 ratio. The “set.seed” function was used in advance of the data division and hyperparameter adjustment of each predictive model to ensure the reproduction of the results. We further divided the training data into smaller sets to estimate the test error associated with a given model (model evaluation) and select the appropriate level of flexibility of the predictive model (selection of the model's hyperparameters). The resampling method adopted was 10-fold cross-validation repeated 5 times.

We tested five algorithms to determine which one returned the best accuracy and precision of the progress of the accumulated sugarcane billbug attack intensity ($AUC_{cumulative}$). The chosen algorithms are random decision trees (called "Random Forest" in this case), support vector machines with radial and polynomial kernels, lasso regression, extreme gradient increasing trees (called "XGBoost"), and sparse partial least squares regression (called "S-PLSR"). These algorithms were selected due to their lower susceptibility to multicollinearity, as observed in data from remote sensing when employing feature selection techniques such as recursive feature elimination commonly used in decision trees, coefficient penalization of insignificant variables such as in lasso regression, and a combination of dimensionality reduction and penalization of uninformative variables like in S-PLS regression (Chen and Guestrin, 2016; Chun and Keleş, 2010; Hengl *et al.*, 2018).

Random Forest and XGBoost algorithms require little preprocessing of predictive variables. For these models, the modification implemented was the creation of "dummy" variables, which is a form of categorical data encoding between 0, symbolizing absence, and 1 as presence. This preprocessing was adopted in the categorical variables as the sampling month and sugarcane varieties. We employed normalization and scaling of numerical variables for the other algorithms, in addition to creating "dummy" variables. The adjustment of the hyperparameters of the models was performed using the function “workflow_map()” contained in the workflow package of the metapackage “tidymodels” in a regular grid of 30 combinations with the “tune_race_anova” function, in which it selects the same candidate parameters from a complete hyperparameter grid while saving time and computational cost (Kuhn and Silge, 2022).

The models were trained and compared to each other to find out which had the highest predictive capacity using the root mean square error metric (RMSE) and determination coefficient (R^2). The model that gave lower RMSE values and a higher R^2 value was selected. From the chosen model, variable importance in projection (VIP) plots were elaborated to visualize the strength of the relationship between each attribute and the observation highlighted by the model in both datasets (UAV and satellite).

Results

Sugarcane billbug damage dynamics, population and cumulative progress of attack

The average values of the proportion of attacked stumps (AS) ranged between 4.9% and 33% AS, depending on variety and sampling month (**Figure 6**). Among the three areas studied, the maximum average value of 33% AS was observed in variety CTC 2994 in the first sampling month, corresponding to December 2022, when the sugarcane was in the tillering phase. The value of 4.9% AS was found in variety RB005014 in the fourth month of assessment (February 2024), during the grand growth phase of the sugarcane. Overall, the AS values decreased in the second and third sampling months and gradually increased afterward. The average biological forms (BFs) displayed a similar pattern to the dynamics found in AS, with a decrease between the second and third months followed by a progressive increase between the fourth and fifth months.

When examining the damage progression curve over the months ($AUC_{cumulative}$), it was observed that the varieties CTC 2994 and CTC 1007 exhibited similar cumulative areas, which were larger than the accumulated damage for RB005014.

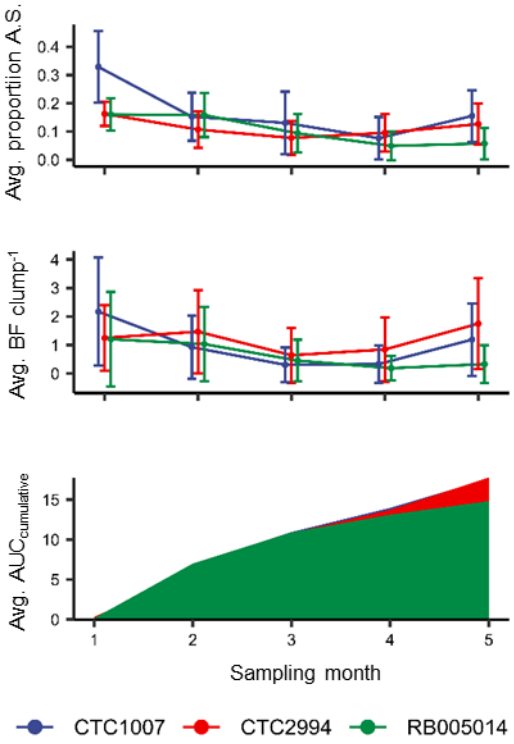


Figure 6 – Average proportion of sugarcane billbug attacked stumps (AS), biological forms (BF: sum of larvae, pupae and adults found inside stumps in the clump) and $AUC_{cumulative}$ by variety (experimental field) and sampling month.

UAV remote sensing

The spectral profile curves of the bands, in relation to infestation levels showed subtle differences between classes (**Figure 7**). The second and third months exhibited the most pronounced differences, with noticeable changes in reflectance magnitude across all bands. Between the fourth and fifth months, the difference in reflectance between classes was less apparent, except for the “Low” class in the fifth month, which showed variation in the red edge and near infrared bands (686, 710, 735, and 850 nm).

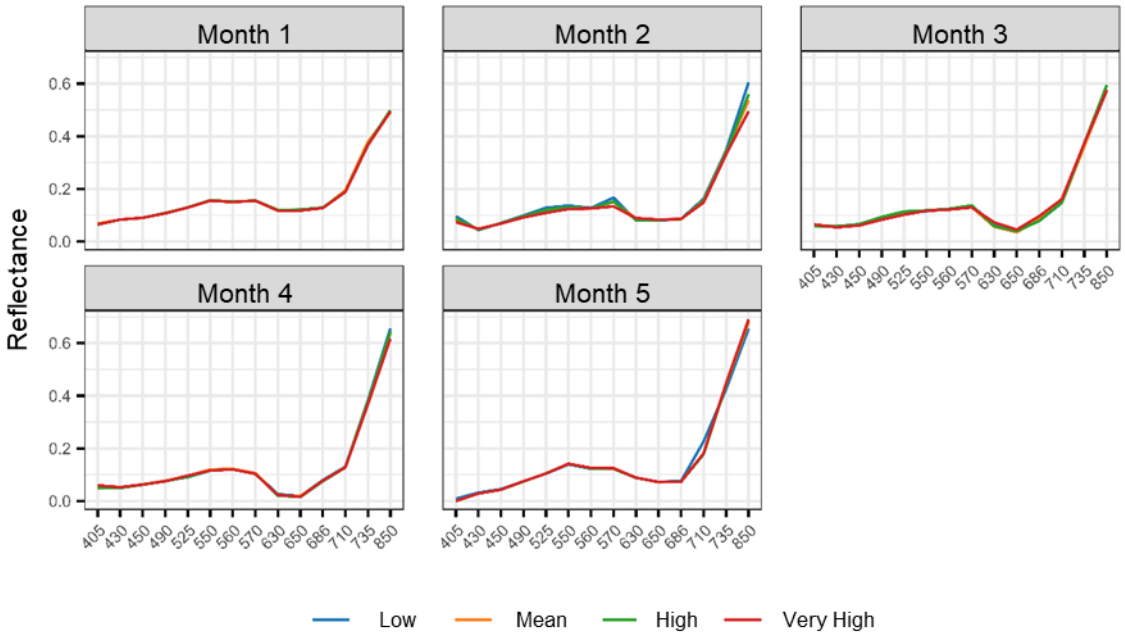
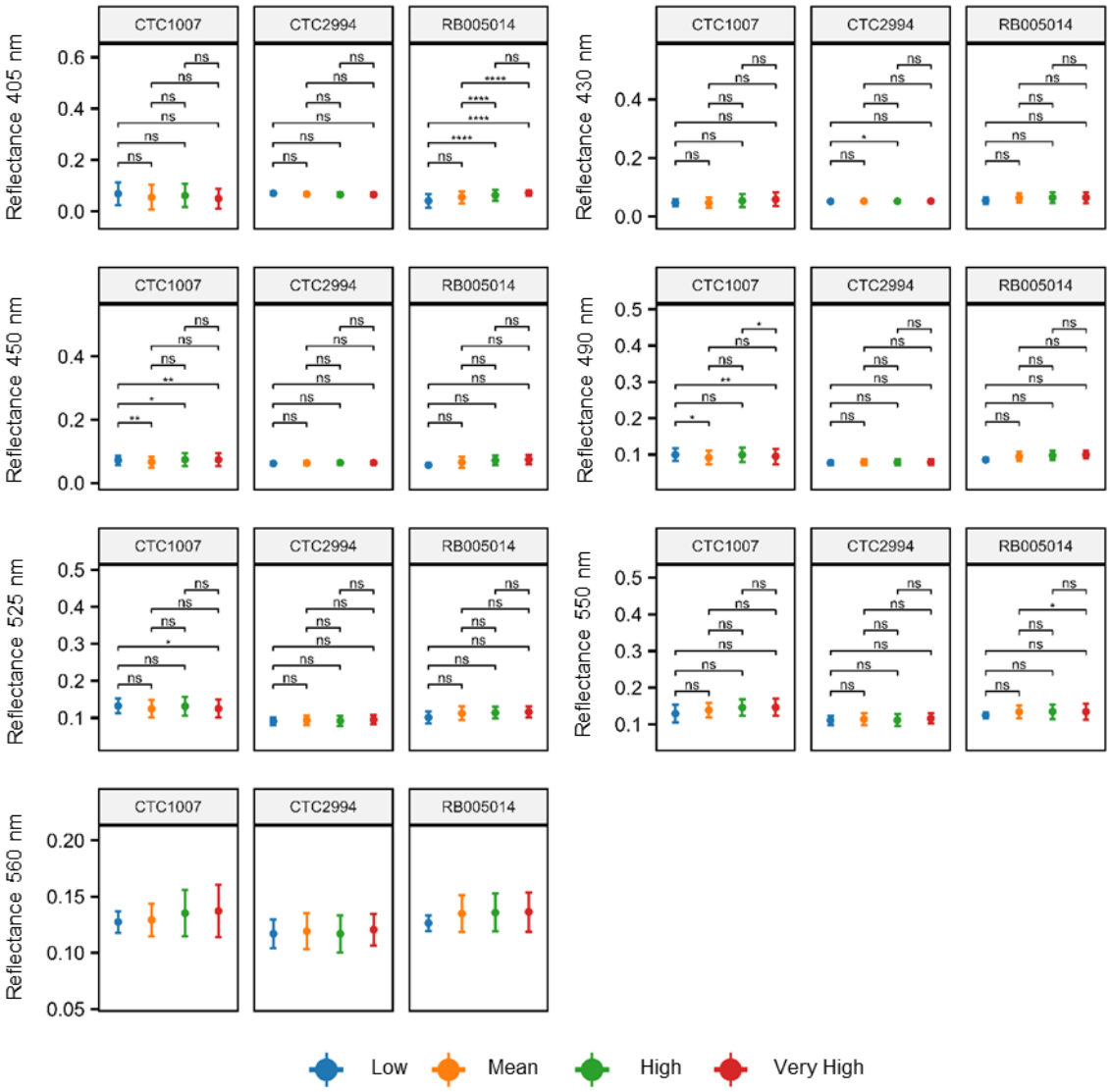


Figure 7 – Average reflectance of the three experimental fields from the Agrowing® sensor. The sugarcane billbug infestation classes were defined from quartiles of the proportion of attacked stumps (Low: 0.0 – 5.6% AS; Mean: 5.7 – 11% AS; High: 11.1 – 18.0% AS; Very high: 18.1 – 75.0% AS).

All bands showed significant differences for at least one factor in the GLMMs (**Table 9**). In some models, the interaction between infestation levels and variety was significant. Where interaction was significant, contrasts highlighted reflectance differences at each infestation level for each variety. For most bands, no significant differences were observed between infestation levels, particularly in bands 560, 630, 650, 686, 710, and 735 nm (**Erro! Fonte de referência não encontrada.**). On the other hand, differences in band reflectance emerged according to the variety and infestation class observed, particularly in bands 405, 430, 450, 490, 525, 550, and 850 nm, with exception of the 570 nm band (**Erro! Fonte de referência não encontrada.**). In general, significant differences were observed between the “Low” and “High” or “Low” and “Very High” categories, with few cases showing differences between “Low” and "Mean”, except for comparisons in variety CTC 1007 for the 450 and 490 nm bands.

Table 9. Wald type 3 test on GLMMs with Student's t distribution family. In the models it was explored whether there are differences in the reflectance extracted from the experimental plots of each band provided by the Agrowing® sensor in function of the sugarcane billbug infestation classes, sugarcane variety, sampling month and interaction between sugarcane billbug infestation classes and variety. In bold are the significant factors at 5% significance

Source of variation	df	Band (nm)													
		405		430		450		490		525		550		560	
		χ^2	P	χ^2	P	χ^2	P	χ^2	P	χ^2	P	χ^2	P	χ^2	P
Intercept	1	$1.81\ 10^4$	**$< 2\ 10^{-16}$**	8316.21	**$< 2\ 10^{-16}$**	5326.93	**$< 2\ 10^{-16}$**	3300.43	**$< 2\ 10^{-16}$**	3185.15	**$< 2\ 10^{-16}$**	3721.51	**$< 2\ 10^{-16}$**	4139.30	**$< 2\ 10^{-16}$**
Infestation class	3	0.77	0.86	1.42	0.70	14.56	$2.23\ 10^{-3}$	14.73	**$2.07\ 10^{-3}$**	9.67	**0.022**	3.82	**0.28**	0.50	0.92
Variety	2	$7.35\ 10^3$	**$< 2\ 10^{-16}$**	13.15	**0.0014**	107.49	**$< 2\ 10^{-16}$**	181.99	**$< 2\ 10^{-16}$**	292.60	**$< 2\ 10^{-16}$**	35.68	**$< 2\ 10^{-16}$**	28.98	**$5.10\ 10^{-7}$**
Sampling month	4	$2.51\ 10^5$	**$< 2\ 10^{-16}$**	4989.68	**$< 2\ 10^{-16}$**	2597.30	**$< 2\ 10^{-16}$**	641.59	**$< 2\ 10^{-16}$**	374.74	**$< 2\ 10^{-16}$**	296.81	**$< 2\ 10^{-16}$**	164.92	**$< 2\ 10^{-16}$**
Infestation class * Variety	6	$2.53\ 10^4$	**$< 2\ 10^{-16}$**	13.74	**0.033**	19.87	**$2.92\ 10^{-3}$**	16.43	**0.012**	11.39	0.077	15.01	**0.020**	4.62	0.59
Source of variation	df	570		630		650		686		710		735		850	
		χ^2	P	χ^2	P	χ^2	P	χ^2	P	χ^2	P	χ^2	P	χ^2	P
Intercept	1	2142.50	**$< 2\ 10^{-16}$**	1132.86	**$< 2\ 10^{-16}$**	1610.64	**$< 2\ 10^{-16}$**	3297.19	**$< 2\ 10^{-16}$**	1227.69	**$< 2\ 10^{-16}$**	1614.38	**$< 2\ 10^{-16}$**	848.72	**$< 2\ 10^{-16}$**
Infestation class	3	8.59	**0.035**	6.87	0.076	3.67	0.30	0.67	0.88	1.20	0.75	0.99	0.80	7.18	0.067
Variety	2	116.29	**$< 2\ 10^{-16}$**	133.18	**$< 2\ 10^{-16}$**	49.63	$1.67\ 10^{-11}$	284.11	**$< 2\ 10^{-16}$**	36.10	**$1.45\ 10^{-8}$**	5.02	0.081	36.93	$9.53\ 10^{-9}$
Sampling month	4	376.34	**$< 2\ 10^{-16}$**	1212.74	**$< 2\ 10^{-16}$**	1647.03	**$< 2\ 10^{-16}$**	1337.05	**$< 2\ 10^{-16}$**	221.20	**$< 2\ 10^{-16}$**	116.63	**$< 2\ 10^{-16}$**	199.19	**$< 2\ 10^{-16}$**
Infestation class * Variety	6	5.98	0.43	12.02	0.062	9.65	0.14	10.39	0.11	6.92	0.33	5.72	0.46	17.91	**$6.46\ 10^{-3}$**


CTC1007
CTC2994
RB005014
Reflectance 405 nm
Reflectance 430 nm
Reflectance 450 nm
Reflectance 490 nm
Reflectance 525 nm
Reflectance 550 nm
Reflectance 560 nm
Low
Mean
High
Very High

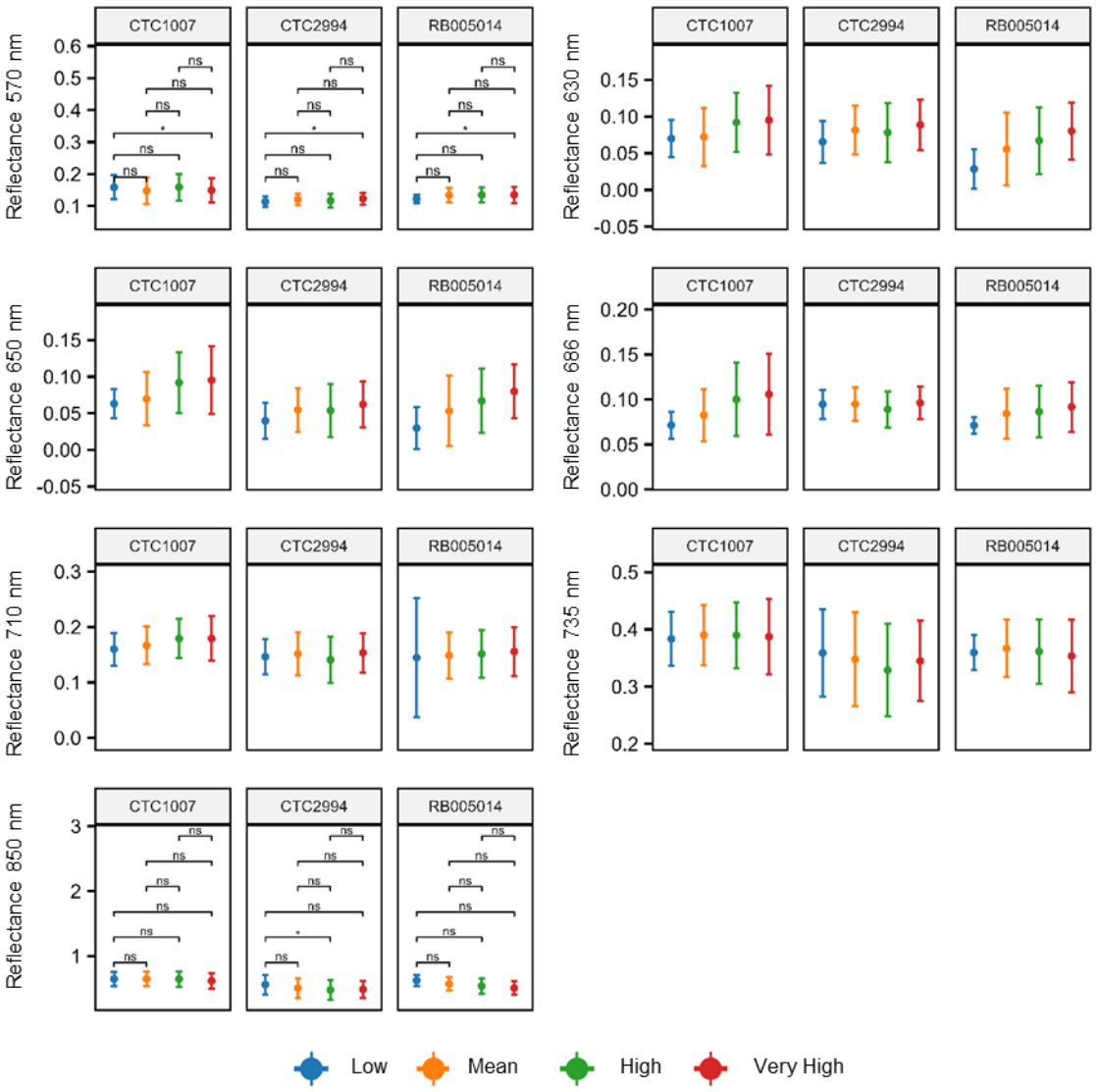


Figure 8 – Comparisons of the reflectance of Agrowing® bands in function of sugarcane billbug infestation classes and sugarcane varieties. Dark circles represent the average, and vertical lines represent the standard deviation. The brackets show the comparison between pairs. *p < 0.05; **p < 0.01; ***p < 0.001; ****p < 0.0001; ns: not significant. Low: 0.0 – 5.6% AS; Mean: 5.7–11% AS; High: 11.1–18.0% AS; Very high: 18.1–75.0% AS.

Decision tree-based algorithms outperformed others (**Table 10**). The Random Forest algorithm achieved the best metrics for the AUC month 1 + month 2 and AUC month 1 + month 2 + month 3 subsets, although its performance was similar to other algorithms such as lasso regression. Among the subsets and algorithms tested with the training data, the combination of AUC month 1 + month 2, predicted by the Random

Forest model, yielded the best metrics, followed by XGBoost, lasso regression, Radial SVM, S-PLS regression, and Polynomial SVM.

Table 10. Model metrics from training data resampling from the Agrowing® sensor. The bold line highlights the selected dataset and model for evaluation in the test data

Dataset	Algorithm	RMSE	R^2
AUC month 1 + month 2	XGBoost	1,88 ± 0,04	0,74 ± 0,01
	Random Forest	**1,87 ± 0,04**	**0,75 ± 0,01**
	Lasso Regression	1,99 ± 0,05	0,71 ± 0,01
	Polinomial SVM	2,02 ± 0,06	0,71 ± 0,02
	Radial SVM	1,98 ± 0,05	0,71 ± 0,02
	S-PLS Regression	1,99 ± 0,05	0,71 ± 0,01
AUC month 1 + month 2 + month 3	XGBoost	2,73 ± 0,05	0,70 ± 0,01
	Random Forest	2,72 ± 0,04	0,70 ± 0,01
	Lasso Regression	2,75 ± 0,05	0,69 ± 0,01
	Polinomial SVM	2,77 ± 0,05	0,69 ± 0,01
	Radial SVM	2,82 ± 0,04	0,68 ±0,01
	S-PLS Regression	2,82 ± 0,06	0,67 ± 0,01
AUC month 1 + month 2+ month 3+ month 4	XGBoost	3,39 ± 0,09	0,65 ± 0,01
	Random Forest	3,30 ± 0,08	0,66 ± 0,02
	Lasso Regression	3,30 ± 0,09	0,66 ± 0,02
	Polinomial SVM	3,32 ± 0,09	0,66 ± 0,02
	Radial SVM	3,45 ± 0,10	0,63 ± 0,01
	S-PLS Regression	3,33 ± 0,08	0,66 ± 0,02
AUC month 1 + month 2 + month 3 + month 4 + month 5	XGBoost	3,65 ± 0,08	0,66 ± 0,01
	Random Forest	3,57 ± 0,08	0,68 ± 0,01
	Lasso Regression	3,56 ± 0,09	0,68 ± 0,01
	Polinomial SVM	3,62 ± 0,09	0,67 ± 0,01
	Radial SVM	3,70 ± 0,09	0,65 ± 0,01
	S-PLS Regression	3,64 ± 0,08	0,67 ± 0,01

Based on the chosen subset data and model, the Random Forest model with optmized hyperparameters (**Table 11**) returned an RMSE of 2.05 and an R^2 of 0.69 on the test data.

Table 11. Configuration of hyperparameters and metrics of the selected Random Forest model in the test data

Dataset	No. trees	Random selected predictors	Minimum node size	RMSE	R^2
AUC month 1 + month 2	500	8	22	2,05	0,69

In this model, a trend of underestimating higher AUC values was observed (**Figure 8 A**). Among the ten predictive variables with the highest importance in the model were observed band reflectance (2), vegetation indices (1), and texture

attributes (7) (**Figure 8 B**). The variables with the greatest impact were the 710 nm band texture correlation and the 430 nm band reflectance.

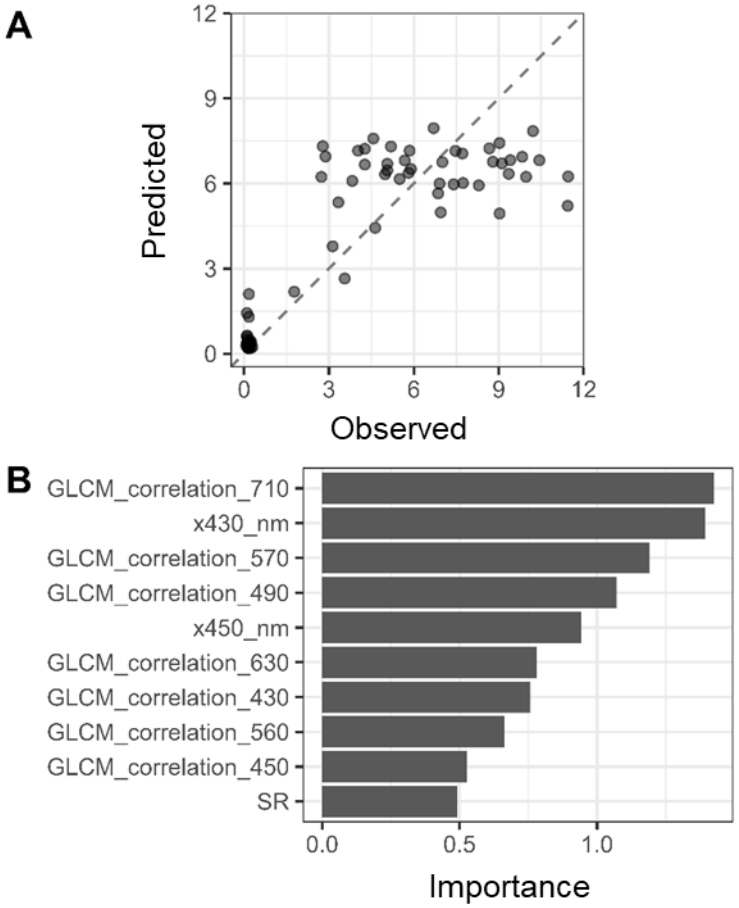


Figure 8 – Predicted vs observed $AUC_{cumulative}$ values in test data and variable importance in projection (VIP) for the Random Forest algorithm.

Orbital remote sensing

The spectral profile curves of Planet® and the Agrowing® sensors showed minimal differences between classes based on sugarcane billbug infestation (**Figure 9**). The variations were observed in the first three months, a period during which there were noticeable changes in the reflectance magnitude across all bands between the evaluated dates and, to a lesser extent, between classes on the same sampling date. The “Very High” infestation class had higher reflectance values than the other classes for the “coastal_blue”, “yellow”, “red” and “red edge” bands. Conversely, the “nir” band initially showed higher reflectance in the first month but lower values for the second and third sampling months. For months 4 and 5, reflectance differences between the classes were negligible.

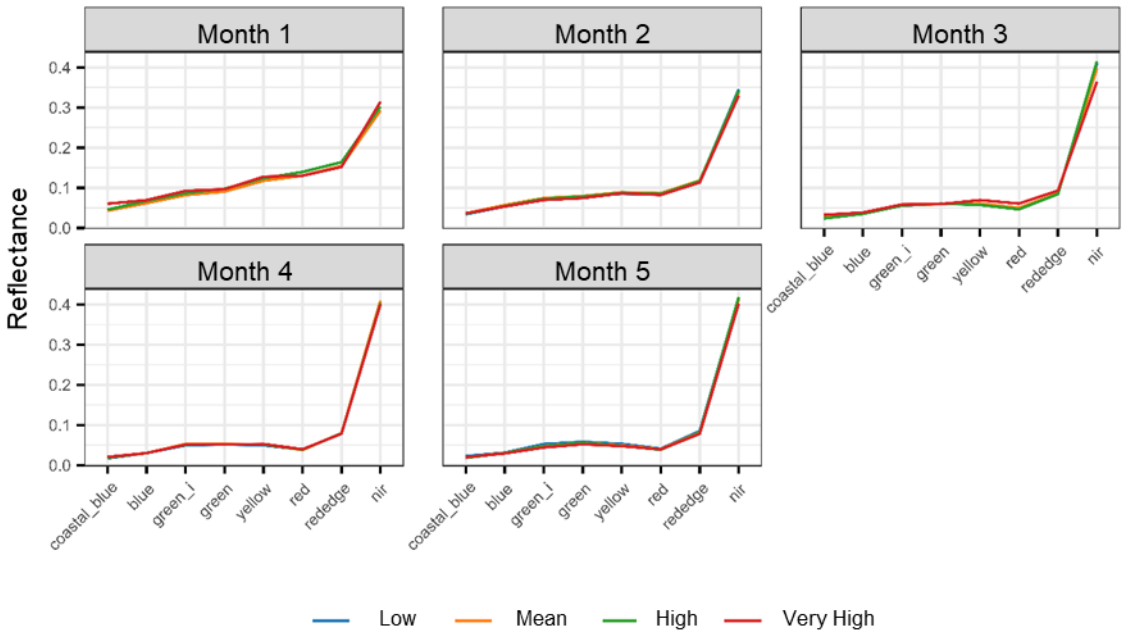


Figure 9 – Average of the reflectance from plots of the three experimental fields. The sugarcane billbug infestation classes were defined from quartiles of the proportion of attacked stumps (Low: 0.0–5.6% AS; Average: 5.7–11% AS; High: 11.1–18.0% AS; Very high: 18.1–75.0% AS).

All bands demonstrated significant differences for at least one factor in the GLMMs (**Table 12**). The models also showed a significant interaction between infestation classes and variety. Therefore, contrasts, explored the reflectance differences for each variety. In general, significant differences between the “Low” and “High” or “Low” and Very High” categories, with few cases showing differences between “Low” and "Mean”, except in variety CTC1007 for the coastal blue, green_i, green, red, and nir bands (). For variety RB005014, there was an increase in reflectance for the yellow, red and red edge bands and a decrease in the nir band when comparing “Low” and “Mean” or other classes.

Table 12. Wald test type 3 on GLMMs with Student t distribution. In the models it was explored whether there are differences in the reflectance extracted from the experimental plots of each band provided by the PlanetScope® constellation in functions of the sugarcane billbug infestation classes, variety, sampling month and interaction between sugarcane billbug infestation classes and variety. In bold are the significant factors at 5% significance

Source of variation	df	Response							
		Coastal_blue		Blue		Green_i		Green	
		χ^2	P	χ^2	P	χ^2	P	χ^2	P
Intercept	1	2153.13	**< 2.2 10^{-16}**	11045.31	**< 2.2 10^{-16}**	8514.92	**< 2.2 10^{-16}**	18926.26	**< 2.2 10^{-16}**
Infestation classes	3	5.39	0.15	9.85	**0.020**	5.78	0.12	9.24	**0.026**
Variety	2	55.37	**9.47 10^{-13}**	50.52	**1.07 10^{-11}**	42.81	**5.06 10^{-10}**	234.18	**< 2.2 10^{-16}**
Sampling month	4	2812.84	**< 2.2 10^{-16}**	5193.61	**< 2.2 10^{-16}**	4508.44	**< 2.2 10^{-16}**	10817.57	**< 2.2 10^{-16}**
Infestation classes * Variety	6	146.72	**< 2.2 10^{-16}**	826.39	**< 2.2 10^{-16}**	228.49	**< 2.2 10^{-16}**	255.44	**< 2.2 10^{-16}**
Source of variation		Yellow		Red		RedEdge		Nir	
		χ^2	P	χ^2	P	χ^2	P	χ^2	P
Intercept	1	9486.82	**< 2.2 10^{-16}**	15494.40	**< 2.2 10^{-16}**	3621.37	**< 2.2 10^{-16}**	11963.70	**< 2.2 10^{-16}**
Infestation classes	3	31.97	**5.30 10^{-7}**	5.88	0.12	17.74	**4.99 10^{-4}**	0.092	0.99
Variety	2	17.79	**1.37 10^{-4}**	198.87	**< 2.2 10^{-16}**	2.51	0.29	630.64	**< 2.2 10^{-16}**
Sampling month	4	10523.37	**< 2.2 10^{-16}**	16170.60	**< 2.2 10^{-16}**	4681.90	**< 2.2 10^{-16}**	85065.89	**< 2.2 10^{-16}**
Infestation classes * Variety	6	190.89	**< 2.2 10^{-16}**	77.53	**1.16 10^{-14}**	106.48	**< 2.2 10^{-16}**	41.60	**< 2.21 10^{-7}**

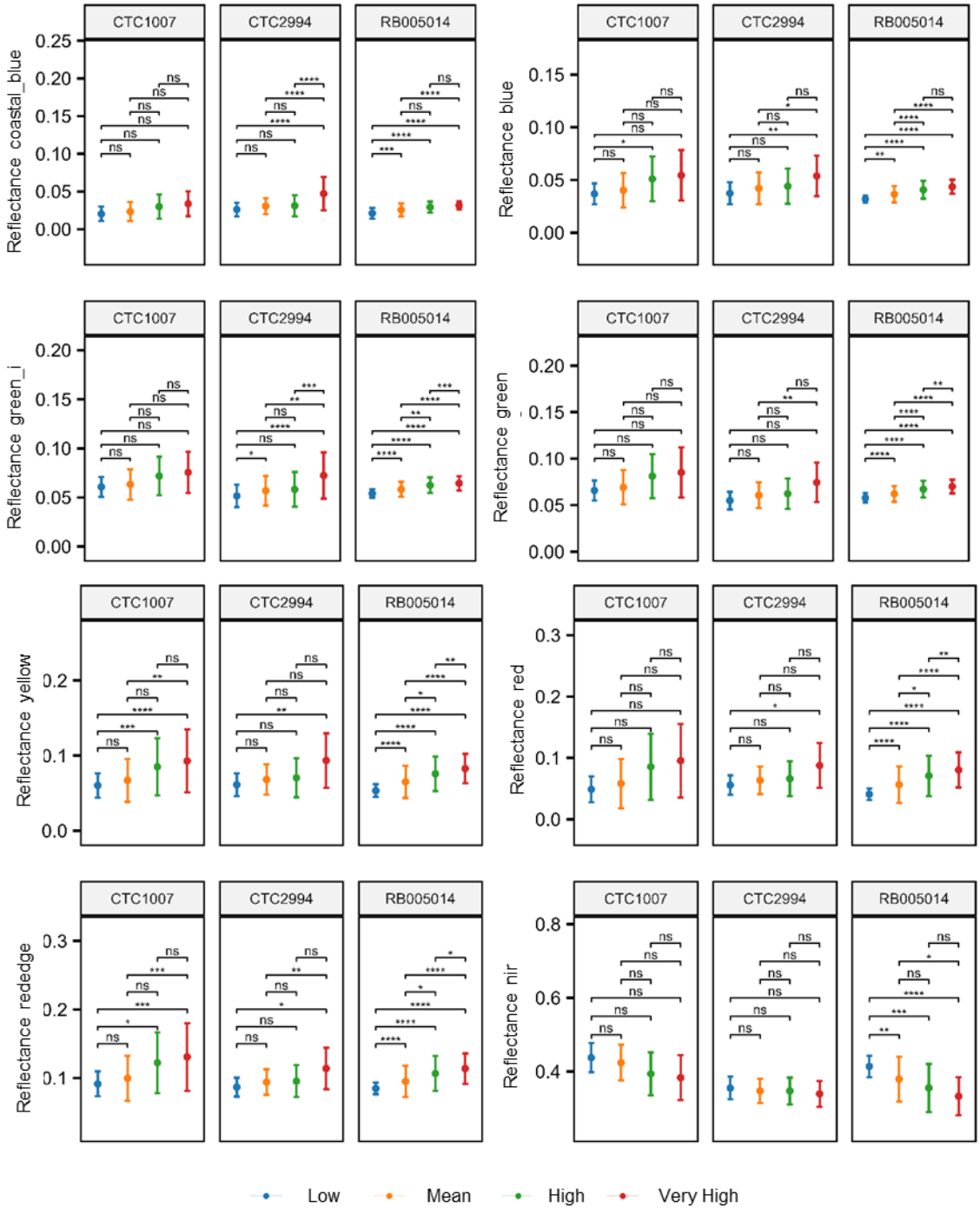


Figure 11 – Comparisons of the Planet® bands according to the sugarcane billbug infestation classes and sugarcane varieties. Dark circles represent the average, and vertical lines represent the standard deviation. The brackets show the comparison between pairs. *p < 0.05; **p < 0.01; ***p < 0.001; ****p < 0.0001; ns: not significant. Low: 0.0–5.6% AS; Mean: 5.7–11% AS; High: 11.1–18.0% AS; Very high: 18.1–75.0% AS.

In all sub-datasets, decision-tree based algorithms also outperformed others (**Table 13**). The XGBoost algorithm achieved better metrics for the AUC month 1 + month 2 and AUC month 1 + month 2 + month 3 datasets, while Random Forest won in the remaining datasets. The subsets and algorithms that performed best with the training data were those that predicted AUC month 1 + month 2 with the XGBoost model, followed by Random Forest, lasso regression, polynomial and radial SVM, and finally S-PLS regression.

Table 13. Model metrics from resampling of training data. The line in bold highlights the selected dataset and model for evaluation in the test data

Dataset	Algorithm	RMSE	R^2
AUC month 1 + month 2	**XGBoost**	**1,68 ± 0,06**	**0,79 ± 0,01**
	Random Forest	1,69 ± 0,06	0,79 ± 0,01
	Lasso Regression	1,70 ± 0,06	0,79 ± 0,01
	Polynomial SVM	1,72 ± 0,06	0,78 ± 0,01
	Radial SVM	1,80 ± 0,06	0,76 ± 0,01
	S-PLS Regression	1,92 ± 0,06	0,73 ± 0,01
AUC month 1 + month 2 + month 3	XGBoost	2,62 ± 0,07	0,74 ± 0,01
	Random Forest	2,65 ± 0,06	0,73 ± 0,01
	Lasso Regression	2,66 ± 0,07	0,73 ± 0,01
	Polynomial SVM	2,67 ± 0,06	0,73 ± 0,01
	Radial SVM	2,69 ± 0,07	0,72 ± 0,01
	S-PLS Regression	2,85 ± 0,07	0,69 ± 0,01
AUC month 1 + month 2+ month 3+ month 4	XGBoost	3,31 ± 0,07	0,70 ± 0,01
	Random Forest	3,25 ± 0,06	0,71 ± 0,01
	Lasso Regression	3,33 ± 0,07	0,69 ± 0,01
	Polynomial SVM	3,37 ± 0,07	0,69 ± 0,01
	Radial SVM	3,40 ± 0,06	0,68 ± 0,01
	S-PLS Regression	3,37 ± 0,06	0,69 ± 0,01
AUC month 1 + month 2 + month 3+ month 4 + month 5	XGBoost	3,90 ± 0,06	0,69 ± 0,01
	Random Forest	3,89 ± 0,06	0,69 ± 0,01
	Lasso Regression	4,07 ± 0,07	0,66 ± 0,01
	Polynomial SVM	4,13 ± 0,06	0,65 ± 0,01
	Radial SVM	4,11 ± 0,06	0,65 ± 0,01
	S-PLS Regression	4,17 ± 0,07	0,64 ± 0,01

Based on the test dataset and selected model with optimized hyperparameters, the XGBoost algorithm (**Table 14**) obtained a RMSE of 1.68 and a R^2 of 0.80 on the test data.

Table 14. Configuration of hyperparameters and metrics of the selected XGBoost model in test data

No. Trees	Tree depth	Random selected predictors	Learning rate	Minimun node size	Loss reduction	Proportion of observed samples	RMSE	R^2
500	2	254	0,00690	26	0,00000000214	0,613	1,68	0,80

Similar to the Random Forest model in the Agrowing® sensor data, the XGBoost model tended to underestimate higher AUC values (**Figure 10 A**). Contributions came from all classes of predictive variables, i.e., including band reflectance (2), vegetation indices (3), PCs (2), and texture attributes (3) (**Figure 10 B**). The most impactful variables were the “red” band and the MCARI vegetation index, with other variables contributing comparatively less.

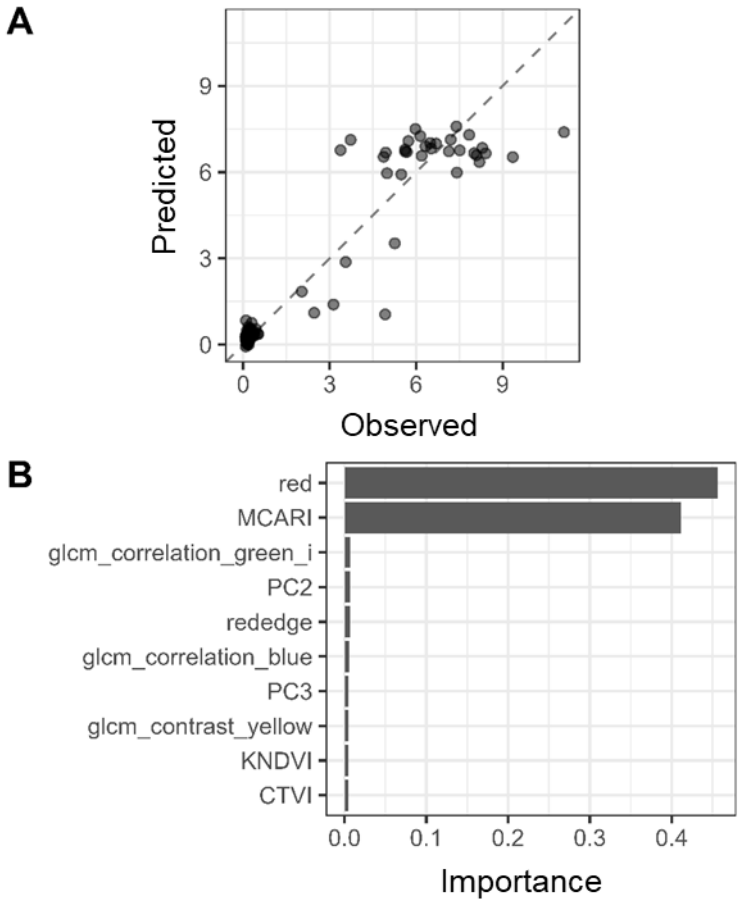


Figure 10 – Predicted vs observed $AUC_{cumulative}$ values (A) and variable importance in projection (VIP) (B) by the XGBoost model in the test data.

Discussion

Multispectral sensors embedded in UAVs and satellites revealed a significant relationship between the spectral reflectance of sugarcane plants and sugarcane billbug infestation classes. Furthermore, in the experimental areas, machine learning models showed satisfactory results in estimating the accumulated attack intensity of the sugarcane billbug during the crop development cycle. Among all datasets and algorithms tested, those representing sugarcane phenology in its tillering phase, preceding intense vegetative growth and full canopy closure and coinciding with the pest's most harmful phase, had better predictive results (lower RMSE and higher R^2) (**Supplementary Figure 1**). This finding emphasizes the importance of prior knowledge of pest bioecology and crop phenology to achieve more effective results.

Insect-induced injuries can cause structural and physiological changes in plants, directly and indirectly affecting plant architecture's spectral reflectance, especially in

the visible and near infrared regions (Nansen and Elliott, 2016; Zhang *et al.*, 2019; Rhodes *et al.*, 2022). However, the response expression of plants, such as the bands that are sensitive and the degree of energy reflection, depends on the injury guild of the stressor (Nansen, 2016; MacRae, Baker and Thompson, 2021). Therefore, bands and vegetation indices sensitive to these changes are assumed to be the most suitable for detecting damage caused by the sugarcane billbug. Nevertheless, our results show that sugarcane varieties respond differently to varying infestation levels. This observation highlights the need to carefully consider future modeling approaches when incorporating new varieties or exploring different modeling methods, such as classification based on infestation level.

Identifying sugarcane billbug damage without collecting the destructive samples poses significant challenges. The primary difficulty refers to injured stems whose symptoms may be confounded with those caused by other stressors, including nematodes *Pratylenchus* spp. (Tylenchida: Pratylenchidae) and other soil pests like *Diloboderus* spp. (Coleoptera: Scarabaeidae, *Migdolus* spp. (Coleoptera: Cerambycidae), and *H. taltula*. In addition, symptoms become more pronounced in intermediate and advanced infestation stages. A recent study suggests that the economic injury level (EIL) of *S. levis* is approximately 5.9% of attacked stumps in sugarcane grown under rainfed conditions (Xavier *et al.*, 2024). Given this threshold, detecting infestation values below the EIL is challenging, as comparisons between the “Low” class, with an upper limit of 5.6% of attacked stumps, and other classes did not reveal significant differences. Economically, late detection is inconvenient, as the resulting damage may be irreversible. In such cases, the grower may lead to additional costs without achieving satisfactory control levels. Early detection of sugarcane billbug, however, may not yield immediate benefits, as pest’s larvae cause the most harm (Dinardo-Miranda, 2005). The larvae, which account for much of the insect's life cycle, remain protected within the sugarcane's culm and root systems, so only the adult stage can be targeted by current control tactics.

Remote sensing-derived datasets can be extensive and highly correlated which may increase overfitting problems in predictive models. To mitigate this issue, we compared learning algorithms that address overfitting internally, employing techniques such as “ensemble” methods (decision trees), penalization in coefficients (lasso regression), and dimensionality reduction (S-PLS regression) (Chun and Keleş, 2010; Belgiu and Drăgu, 2016; Muthukrishnan and Rohini, 2017). Notably, decision trees

stand out with the best predictive capabilities, being less prone to excessive adjustments and capable of handling large-scale data, with a stronger noise tolerance than other algorithms (Belgiu e Drăgu, 2016). However, in both datasets, the winning model tended to underestimate higher AUC values possibly due to the low number of observations found at $AUC_{cumulative} > 10$. Incorporating more extreme observations could improve models performance by better capturing the predictive variable patterns (Hastie, Tibshirani and Friedman, 2009). Data fusion combining data from multiple sources for greater accuracy, is another promising approach (Barbedo, 2022). Since insects depend on abiotic factors for their life cycle, including temperature and humidity, environmental data may help enhance predictions (Régnière *et al.*, 2012; Abarca and Spahn, 2021). For this purpose, soil-embedded temperature and humidity sensors could be used for data collection to infer favoring sugarcane billbug development.

The variable importance in projection (VIP) analysis varied by sensor. For Agrowing®, the 710 nm band correlation and 450 nm band reflectance emerged as key variables. Various studies have reported enhanced pest and disease detection through texture analysis (Zhou *et al.*, 2017; Barman, Pathak and Mazumder, 2023; Kabir *et al.*, 2024). Texture extraction can segment images and reveal regions with likely sugarcane billbug infestation (Barman, Pathak and Mazumder, 2023). Moreover, the sugarcane billbug injury in rhizomes may compromise water absorption, resulting in water stress. Pest infestations can also reduce chlorophyll, which strongly absorbs in the blue and red spectrum, causing higher reflectance in the blue region. Meanwhile, the MCARI vegetation index and the "red" band stood out as significant predictors highlighted by the VIP in the Planet® data. MCARI provides a measurement of the depth of chlorophyll absorption and is sensitive to variations in concentration as well as changes in the index of foliar area (IAF), minimizes the impact of lighting conditions, soil background reflection, and other non-photosynthetic elements (Daughtry *et al.*, 2000). This feature is advantageous, as sugarcane during the sprouting phase, as in the winning dataset, retains significant straw cover on soil surface. The “red” band, like the blue band, relates to energy absorption in photosystems, with stressed plants reflecting more energy in this region. Both predictors hold biological significance, as sugarcane billbug-attacked plants exhibit yellowing of older leaves. In young plants, pest attacks may reduce sugarcane tiller density, impacting canopy cover and, thus, leaf area index. This suggests that sugarcane billbug affects photosynthetic capacity

of sugarcane plants by destroying the conductive vessels, interrupting water and nutrient flow from the root system to the aerial organs. Unlike defoliating insects, the sugarcane billbug attacks the culm base and rhizome, imposed prolonged damage to the vascular system (Zvereva and Kozlov, 2012).

Orbital images offer advantages over UAV imaging, including no need for costly equipment and software, travel to field sites, and broader area coverage for a comprehensive view of the problem (Zhang *et al.*, 2016). Limitations include longer revisiting times and lower spectral and spatial resolution, depending on the satellite constellation and the proposed target objective (Messina *et al.*, 2020; Trubin *et al.*, 2023). Some of these constraints are mitigated by constellations such as PlanetScope®, which provides near daily images with high spatial resolution (~3.5 m) in up to eight bands of the visible and near-infrared spectrum bands (Planet Labs, 2024). Unexpectedly, the performance of predictive models based on the Planet dataset outperformed those from the Agrowing® sensor. Typically, UAV data surpasses satellite data in model performance (Khaliq *et al.*, 2019; Awais *et al.*, 2022). This observation may stem from removing background pixels in UAV data processing prior to information extraction. However, Planet data did not exclude soil pixels, given the spatial resolution is exceeded the row spacing. This likely underscores the importance of overall leaf area for accurately detecting billbug damage, beyond plant response alone.

This study marks the first use of aerial and orbital remote sensing to detect sugarcane stress associated with sugarcane billbug infestations. Satellite images stand out for their predictive power and have proved to be a promising tool for monitoring *S. levis*. Satellites offer greater terrestrial coverage than other remote detection technologies, which can increase the efficiency of regional sugarcane billbug surveillance. However, crediting sugarcane billbug infestation through remote sensing is still a tough task. Many stressors may impose similar spectral responses in sugarcane plants and require field confirmation. Thus, areas possibly attacked by *S. levis* and detected by the images can identify hot spots and direct a team of scouters in the field for confirmation of the anomaly cause. Such results represent a first step toward improving a large-scale monitoring scheme for the sugarcane billbug.

References

ABARCA, M.; SPAHN, R. Direct and indirect effects of altered temperature regimes and phenological mismatches on insect populations. **Current Opinion in Insect Science**, v. 47, p. 67–74, 2021.

ALENCAR, J. R. D. C. C. **Dinâmica populacional, distribuição espacial e plano de amostragem sequencial de *Sphenophorus levis* Vaurie, 1978 (Coleoptera: Curculionidae) em cana-de-açúcar**. Jaboticabal, SP: Universidade Estadual Paulista, Faculdade de Ciências Agrárias e Veterinárias, 2016.

ALVES, D. P.; TOMAZ, R. S.; LAURINDO, B. S.; LAURINDO, R. D. F.; E SILVA, F. F.; CRUZ, C. D.; NICK, C.; SILVA, D. J. H. DA. Artificial neural network for prediction of the area under the disease progress curve of tomato late blight. **Scientia Agricola**, v. 74, n. 1, p. 51–59, 2017.

AWAIS, M.; LI, WEI; HUSSAIN, S.; CHEEMA, M. J. M.; LI, WEIGUO; SONG, R.; LIU, C. Comparative evaluation of land surface temperature images from unmanned aerial vehicle and satellite observation for agricultural areas using in situ data. **Agriculture**, v. 12, n. 2, p. 184, 2022.

BARBEDO, J. G. A. A review on the use of unmanned aerial vehicles and imaging sensors for monitoring and assessing plant stresses. **Drones**, v. 3, n. 2, p. 40, 2019.

BARBEDO, J. G. A. Data fusion in agriculture: resolving ambiguities and closing data gaps. **Sensors**, v. 22, n. 6, p. 2285, 2022.

BARMAN, U.; PATHAK, C.; MAZUMDER, N. K. Comparative assessment of pest damage identification of coconut plant using damage texture and color analysis. **Multimedia Tools and Applications**, v. 82, n. 16, p. 25083–25105, 2023.

BELGIU, M.; DRĂGU, L. Random forest in remote sensing: a review of applications and future directions. **ISPRS Journal of Photogrammetry and Remote Sensing**, v. 114, p. 24–31, 2016.

BROOKS, M. E.; KRISTENSEN, K.; BENTHEM, KOEN, J., V.; MAGNUSSON, A.; BERG, CASPER, W.; NIELSEN, A.; SKAUG, HANS, J.; MÄCHLER, M.; BOLKER, BENJAMIN, M. glmmTMB balances speed and flexibility among packages for zero-inflated generalized linear mixed modeling. **The R Journal**, v. 9, n. 2, p. 378–400, 2017.

CHEN, T.; GUESTRIN, C. XGBoost: a scalable tree boosting system. **Proceedings of the ACM SIGKDD International Conference on Knowledge Discovery and Data Mining**, p. 785–794, 2016.

CHUN, H.; KELEŞ, S. Sparse partial least squares regression for simultaneous dimension reduction and variable selection. **Journal of the Royal Statistical Society Series B: Statistical Methodology**, v. 72, n. 1, p. 3–25, 2010.

DARA, S. K. The new Integrated Pest Management paradigm for the modern age. **Journal of Integrated Pest Management**, v. 10, n. 1, 2019.

DAUGHTRY, C. S. T.; WALTHALL, C. L.; KIM, M. S.; COLSTOUN, E. B.; MCMURTREY III, J. E. Estimating corn leaf chlorophyll concentration from leaf and canopy reflectance. **Remote Sensing of Environment**, v. 74, n. 2, p. 229–239, 2000.

DINARDO-MIRANDA, L. L. Nematóides e pragas de solo em cana-de-açúcar. **Informações agronômicas nº 110**, v. 1, p. 25–32, 2005.

HARALICK, R. M.; SHANMUGAM, K.; DINSTEIN, I. Textural features for image classification. **IEEE Transactions on Systems, Man, and Cybernetics**, v. SMC-3, n. 6, p. 610–621, 1973.

HARTIG, F. **DHARMa: Residual Diagnostics for hierarchical (multi-level / mixed) regression models**, 2022. Disponível em: <https://CRAN.R-project.org/package=DHARMa>

HASTIE, T.; TIBSHIRANI, R.; FRIEDMAN, J. **The elements of statistical learning**. 2. ed. New York, NY: Springer New York, 2009.

HENGL, T.; NUSSBAUM, M.; WRIGHT, M. N.; HEUVELINK, G. B. M.; GRÄLER, B. Random forest as a generic framework for predictive modeling of spatial and spatio-temporal variables. **PeerJ**, v. 6, p. e5518, 29 ago. 2018.

HIGLEY, L.; PEDIGO, L. **Economic thresholds for integrated pest management**. Nebraska, USA: University of Nebraska Press, 1996.

ILICH, A. R. **GLCMTextures**, 2020. Disponível em: <https://github.com/ailich/GLCMTextures.>. Acesso em: 3 fev. 2024

KABIR, M.; UNAL, F.; AKINCI, T. C.; MARTINEZ-MORALES, A. A.; EKICI, S. Revealing GLCM metric variations across a plant disease dataset: a comprehensive examination and future prospects for enhanced deep learning applications. **Electronics**, v. 13, n. 12, p. 2299, 2024.

KARIMZADEH, R.; SCIARRETTA, A. Spatial patchiness and association of pests and natural enemies in agro-ecosystems and their application in precision pest management: a review. **Precision Agriculture**, v. 23, n. 5, p. 1836–1855, 2022.

KHALIQ, A.; COMBA, L.; BIGLIA, A.; RICAUDA AIMONINO, D.; CHIABERGE, M.; GAY, P. Comparison of satellite and UAV-based multispectral imagery for vineyard variability assessment. **Remote Sensing**, v. 11, n. 4, p. 436, 2019.

KUHN, M.; SILGE, J. **Tidy modeling with R: a framework for modeling in the tidyverse**. 1. ed. Massachusetts, USA: O'Reilly Media Inc, 2022.

KUHN, M.; WICKHAM, H. **Tidymodels: a collection of packages for modeling and machine learning using tidyverse principles.**, 2020. Disponível em: <https://www.tidymodels.org>. Acesso em: 15 maio. 2024

LEUTNER, B.; HORNING, N.; SCHWALB-WILLMANN, J.; MUELLER, K. **RStoolbox: remote sensing data analysis**, 2024. Disponível em: <https://CRAN.R-project.org/package=RStoolbox>

MACRAE, I.; BAKER, T.; THOMPSON, A. Notes on UAS and remote sensing of insect damage. **American Journal of Potato Research**, v. 98, n. 1, p. 16–23, 2021.

MAHANTA, D. K.; BHOI, T. K.; KOMAL, J.; SAMAL, I.; MASTINU, A. Spatial, spectral and temporal insights: harnessing high-resolution satellite remote sensing and artificial intelligence for early monitoring of wood boring pests in forests. **Plant Stress**, v. 11, p. 100381, 2024.

MESSINA, G.; PEÑA, J. M.; VIZZARI, M.; MODICA, G. A comparison of UAV and satellites multispectral imagery in monitoring onion crop. An application in the 'Cipolla Rossa di Tropea' (Italy). **Remote Sensing**, v. 12, n. 20, p. 3424, 2020.

MUTHUKRISHNAN, R.; ROHINI, R. LASSO: a feature selection technique in predictive modeling for machine learning. **2016 IEEE International Conference on Advances in Computer Applications, ICACA 2016**, p. 18–20, 2017.

NANSEN, C. The potential and prospects of proximal remote sensing of arthropod pests. **Pest Management Science**, v. 72, n. 4, p. 653–659, 2016.

NANSEN, C.; ELLIOTT, N. Remote sensing and reflectance profiling in entomology. **Annual Review of Entomology**, v. 61, n. 1, p. 139–158, 2016.

OLIVOTO, T. Lights, camera, pliman! An R package for plant image analysis. **Methods in Ecology and Evolution**, v. 13, n. 4, p. 789–798, 2022.

PAVLU, F. A.; MOLIN, J. P. Plano de amostragem e distribuição espacial para controle localizado de <i>Sphenophorus levis<i/> em cana-de-açúcar. **Acta Scientiarum - Agronomy**, v. 38, n. 3, p. 279–287, 2016.

PAVLU, F. A.; MOLIN, J. P.; PAVLU, F. A.; MOLIN, J. P. A sampling plan and spatial distribution for site-specific control of *Sphenophorus levis* in sugarcane. **Acta Scientiarum. Agronomy**, v. 38, n. 3, p. 279, 2016.

PETERSON, R. K. D.; HIGLEY, L. G.; PEDIGO, L. P. Whatever happened to IPM? **American Entomologist**, v. 64, n. 3, p. 146–150, 2018.

PLANET LABS, INC. **Real-time satellite monitoring with Planet**. Disponível em: <https://www.planet.com/products/satellite-monitoring/>. Acesso em: 3 jul. 2024.

PRETI, M.; VERHEGGEN, F.; ANGELI, S. Insect pest monitoring with camera-equipped traps: strengths and limitations. **Journal of Pest Science**, v. 94, n. 2, p. 203–217, 2021.

R CORE TEAM. **R: a language and environment for statistical computing**. Disponível em: <https://www.R-project.org/>.

REAGAN, T. E.; MULCAHY, M. M. Interaction of cultural, biological, and varietal controls for management of stalk borers in Louisiana sugarcane. **Insects**, v. 10, n. 9, p. 305, 2019.

RÉGNIÈRE, J.; POWELL, J.; BENTZ, B.; NEALIS, V. Effects of temperature on development, survival and reproduction of insects: experimental design, data analysis and modeling. **Journal of Insect Physiology**, v. 58, n. 5, p. 634–647, 2012.

RHODES, M. W.; BENNIE, J. J.; SPALDING, A.; FFRENCH-CONSTANT, R. H.; MACLEAN, I. M. D. Recent advances in the remote sensing of insects. **Biological Reviews**, v. 97, n. 1, p. 343–360, 2022.

ROSA, J. O.; SOARES, J. R. S.; FERNANDES, O. A. Harvest load transfer sites influence sugarcane billbug (Coleoptera: Curculionidae) spatiotemporal injury in sugarcane. **Pest Management Science**, v. 80, n. 4, p. 1771–1778, 2024.

RUPPEL, R. F. Model for effective timing of an insecticide. **Journal of Economic Entomology**, v. 77, n. 5, p. 1083–1085, 1984.

SILVA, A. R. DA; TAVARES FILHO, I. J.; GONÇALVES DE JESUS, F.; SOUSA ALMEIDA, A. C. DE. On monitoring *Mahanarva fimbriolata* Stål (Hemiptera: Cercopidae) in sugarcane fertirrigated with vinasse. **Sugar Tech**, v. 25, n. 1, p. 245–249, 2023.

SMITH, G. M.; MILTON, E. J. The use of the empirical line method to calibrate remotely sensed data to reflectance. **International Journal of Remote Sensing**, v. 20, n. 13, p. 2653–2662, 1999.

T2R SOLUÇÕES TECNOLÓGICAS. **T2R Geotagger.**Presidente Prudente, 2024.

TRUBIN, A.; KOZHORIDZE, G.; ZABIHI, K.; MODLINGER, R.; SINGH, V. V.; SUROVÝ, P.; JAKUŠ, R. Detection of susceptible Norway spruce to bark beetle attack using PlanetScope multispectral imagery. **Frontiers in Forests and Global Change**, v. 6, p. 1130721, 2023.

VANEGAS, F.; BRATANOV, D.; WEISS, J.; POWELL, K.; GONZALEZ, F. Multi and hyperspectral UAV remote sensing: grapevine phylloxera detection in vineyards. **2018 IEEE Aerospace Conference**, p. 1–9, mar. 2018.

XAVIER, G. G.; SÁ FARIAS, E. DE; CARMO, D. DAS G. DO; GUEDES, A. G.; SAMUELS, R. I.; FREITAS, D. R. DE; PEREIRA, E. J. G.; LIMA, E.; PICANÇO, M. C. Determining factors and economic injury levels for *Sphenophorus levis* for chemical and biological control in irrigated and non-irrigated sugarcane crops. **Neotropical Entomology**, 2024.

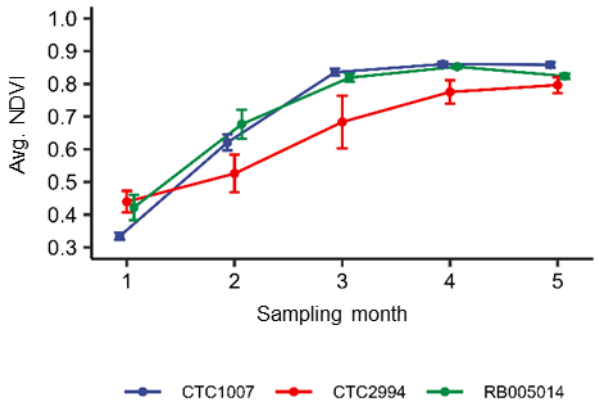
ZHANG, J.; HUANG, Y.; PU, R.; GONZALEZ-MORENO, P.; YUAN, L.; WU, K.; HUANG, W. Monitoring plant diseases and pests through remote sensing technology: a review. **Computers and Electronics in Agriculture**, v. 165, p. 104943, 2019.

ZHANG, J.; HUANG, Y.; YUAN, L.; YANG, G.; CHEN, L.; ZHAO, C. Using satellite multispectral imagery for damage mapping of armyworm (*Spodoptera frugiperda*) in maize at a regional scale. **Pest Management Science**, v. 72, n. 2, p. 335–348, 2016.

ZHOU, C.; LEE, W. S.; ZHANG, S.; LIBURD, O. E.; POURREZA, A.; SCHUELLER, J. K.; AMPATZIDIS, Y. A smartphone application for site-specific pest management based on deep learning and spatial interpolation. **Computers and Electronics in Agriculture**, v. 218, p. 108726, 1 mar. 2024.

ZHOU, J.; YAN GUO, R.; SUN, M.; DI, T. T.; WANG, S.; ZHAI, J.; ZHAO, Z. The effects of GLCM parameters on LAI estimation using texture values from Quickbird satellite imagery. **Scientific Reports**, v. 7, n. 1, p. 7366, 2017.

ZVEREVA, E. L.; KOZLOV, M. V. Sources of variation in plant responses to belowground insect herbivory: a meta-analysis. **Oecologia**, v. 169, n. 2, p. 441–452, 2012.



Supplementary Figure 1 – Average of the NDVI (Normalized Difference Vegetation Index) of the plots from each experimental area and evaluation month extracted from the PlanetScope® constellation. Circles and error bars represent the average and standard deviation, respectively. The lines show how much the experimental areas evolved in biomass, where the sugarcane varieties RB005014 and CTC 1007 reached their peak in the third month and the variety CTC 2994 in the fourth month.

CHAPTER 4 – Concluding remarks

Studies on insect-plant interactions help us understand how plants respond to pest attacks and identify critical moments for intervention. This knowledge is essential for minimizing agricultural losses and developing decision-making indices, such as the Economic Injury Level (EIL) and Action Threshold (AT). However, the level of complexity may increase when considering interactions with other biotic or abiotic factors. This complexity may bring a more cautious approach, as it can intensify plant stress and potentially lead to greater losses, underscoring the need to refine decision-making indices. The results of this research reveal that there are no synergies between the attack of the sugarcane borer and moderate water stress on gas exchange parameters and leaf spectral reflectance of sugarcane plants. In future studies, it would be interesting to explore possible compensatory mechanisms that plants trigger in response to pest attacks and, if possible, isolate the indirect effects caused by fungi responsible for red rot in culms. Additionally, it would be relevant to explore sugarcane's ability to tolerate the attack of boring insects.

Digital agricultural tools have driven new solutions to advance decision-making. The limited workforce and high costs are listed as major obstacles for implementing large-scale IPM programs. Thus, apps, IoT devices, and remote sensing bring new opportunities to address this problem. A key advantage is the creation of a robust infestation history, which can later become crucial to understanding the complex ecological processes of pests. In the case of sugarcane billbugs, the current sampling plan requires scouters to dig up the sugarcane clumps and cut the remnants of harvested culms to account for attacked stumps and biological forms. Besides being a demanding task, the current scheme introduces inherent risks, exposing scouters to cutting tools and venomous animals, making it challenging to recruit new workers. This has led to an increase in employee turnover and a shortage of scouts available to do this type of work.

This study contributes to a pioneering initiative for sampling sugarcane billbug through remote sensing to accelerate pest infestation data collection in sugarcane fields and reduce the need for human intervention. As part of improving the monitoring of the sugarcane billbug through remote sensing, the results reveal the importance of bands in the visible spectrum bands, vegetation indices, and image texture attributes related to billbug attack. Data from multispectral sensors on satellites showed better

results than those recorded by UAVs. Furthermore, sugarcane phenology plays a significant role in detecting pest attacks, with algorithms providing more accurate predictions of accumulated pest infestations when sugarcane has not yet reached its maximum leaf area. Despite the insights gained, significant challenges remain. One challenge is correctly identifying the stressor, which may have similar reflectance characteristics. It is crucial to emphasize that the search for images or other variables in the context of digital agriculture, that can verify a plant's response to the biotic stressor (insect pest) and confirm its presence, is both current and necessary. However, there are still very few successful cases in literature. Consequently, monitoring implementation remains challenging, and on-site confirmation is still required. Meanwhile, digital monitoring can guide field scout teams to suspected areas with higher infestations, thus improving resource efficiency and speeding up decision-making.